

**Multi-scale Observations of Atmospheric Moisture Variability in relation to Heavy
Precipitating Systems in the north-western Mediterranean during HyMeX IOP12**

¹S. Khodayar, ¹B. Czajka, ¹A. Caldas-Alvarez, ¹S. Helgert, ²C. Flamant, ³P. Di Girolamo, ⁴O.
Bock, ⁵P. Chazette

¹Institute of Meteorology and Climate Research (IMK-TRO), Karlsruhe Institute of
Technology (KIT), Karlsruhe, Germany

²LATMOS/IPSL, UPMC Univ. Paris 06 Sorbonne Universités, UVSQ, CNRS, Paris, France

³Scuola di Ingegneria, Università della Basilicata, Via dell'Ateneo Lucano n. 10, 85100
Potenza, Italy.

⁴IGN LAREG, Univ. Paris Diderot, Sorbonne Paris Cité, 5 rue Thomas Mann, 75205 Paris
CEDEX 13, France

⁵Laboratoire des Sciences du Climat et de l'Environnement, CEA-CNRS-UVSQ, Gif-sur-
Yvette, France

* Corresponding author. E-mail address: samiro.khodayar@kit.edu (S. Khodayar)

Institute for Meteorology and Climate Research, Karlsruhe Institute of Technology
(KIT), Postfach 3640, 76021 Karlsruhe, Germany

This article has been accepted for publication and undergone full peer review but has not
been through the copyediting, typesetting, pagination and proofreading process, which
may lead to differences between this version and the Version of Record. Please cite this
article as doi: 10.1002/qj.3402

Abstract

The deployment of special instrumentation for the Hydrological Cycle in the Mediterranean Experiment (HyMeX) provides a valuable opportunity to investigate the spatio-temporal variability of atmospheric water vapour across scales in relationship with the occurrence of Heavy Precipitation Systems (HPSs) in the north-western Mediterranean (WMed) during the Intensive Observation Period (IOP12), which is the focus of this investigation. High-resolution convective permitting COSMO simulations complement the observational network and allow the calculation of online trajectories.

In addition to the presence of a favourable large-scale situation and low-level convergence, atmospheric moisture changes resulting in conditionally unstable air are identified as responsible for convective initiation (CI). All HPSs within the north-WMed form in periods/areas of maximum Integrated Water Vapour (IWV; $35\text{-}45 \text{ kg m}^{-2}$) after an increase of about $10\text{-}20 \text{ kg m}^{-2}$. The most intense events receive moisture from different sources simultaneously and show a sudden increase of about 10 kg m^{-2} between 6-12 h prior to the event, whereas in the less intense events the increase is larger, about 20 kg m^{-2} , over a period of at least 24 h-36 h. Changes in the lower ($\sim 900 \text{ hPa}$) and mid-troposphere ($\sim 700 \text{ hPa}$) control the evolution of the atmospheric moisture and the instability increase prior to CI. Spatial inhomogeneities in the lower boundary layer determine the timing and location of deep convection, whereas enhanced moisture in the mid-troposphere favours intensification. Moister and deeper boundary layers, with updraughts reaching up to 2 km are identified in those pre-convective environments leading to HPS, whereas dry, shallow boundary layers are found everywhere else. The build-up time and vertical distribution of the moisture changes are found to be crucial for the evolution and severity of the HPSs rather than the amount of total column atmospheric moisture.

Key Words: HyMeX, Heavy Precipitation System, convection, multi-scale water vapour variability, observations

1. Introduction

Every year, the Mediterranean region is affected by high impact weather mainly in the form of Heavy Precipitation Systems (HPSs). These come often in the form of severe storms bringing, in addition to heavy precipitation and flooding, strong wind gusts, intense lightning, large hail and even tornadoes. Most of the HPSs with the accompanying flash floods occur between September and November and are caused mainly by Mesoscale Convective Systems (MCSs; Riosalido 1990).

Although the large-scale processes governing the occurrence of convection producing HPSs in the western Mediterranean (WMed) have long been studied and are generally well understood (e.g. Nuissier et al. 2008), there still are open questions concerning the role of enhancing factors affecting the initiation, the development, the type or the severity of convective storms. Among these, atmospheric water vapour is crucial for the occurrence of deep convection.

It is well known that besides a triggering mechanism, large-scale lifting and/or low level convergence allowing the release of the potential energy, small convective inhibition, and an conditionally unstable atmosphere, the main ingredient required for the occurrence of deep convection is a moist atmosphere (Doswell et al. 1996). Particularly relevant is the presence of sufficient moisture in the low- and mid-troposphere (e.g. Khodayar et al 2010, 2013). The availability of moisture for precipitation is controlled by a number of processes including

mixing on small scales, convective processes on different scales, and advection on the mesoscale and large-scale.

Former studies (e.g. Nuissier et al. 2011) pointed out that HPSs in the WMed often occur under the influence of a synoptic pattern that is quasi-stationary in time and favours a steady low-level moist flow towards the coast. This transport of moisture provides the large amounts of water vapour needed to feed the precipitating systems producing huge quantities of precipitation recorded during these events. Modelling studies in the last years also suggest that the main moisture sources for HPSs in the north-WMed are evaporation from North Africa, the Mediterranean and the Atlantic (e.g. Winschall et al. 2012; Duffourg and Ducrocq 2013; Ramos et al. 2016). The time scale of the moisture transport was assessed to be about 2 days for local sources, and 2 to 5 for contributions from the Tropics. Few observational investigations have been conducted to confirm these results (e.g. Chazette et al. 2016a; Lee et al. 2016). Furthermore, humidity shows large spatial and temporal variability on the mesoscale (Crook 1996; Lauscaux et al. 2004; Weckwerth et al. 1996, 2000; Khodayar et al. 2010, 2013, 2016a). The small-scale variations of humidity can directly influence convective initiation (CI), as well as its further development potential (Sherwood et al. 2010). Moisture variations of about 1 g kg^{-1} in the Planetary Boundary Layer (PBL) can make the difference between no initiation and intense convection (Crook 1996). Weckwerth et al. (1996) showed that this magnitude of variability occurs regularly in the PBL on distances of a few kilometres only.

The combination of the various processes and scales discussed above results in a high variability in both space and time, whose exact knowledge is essential for both Numerical Weather Prediction (NWP; e.g. Weckwerth et al. 1999) and climate modelling (e.g. Bony et al. 2006). Advances have been achieved in the last years concerning convective processes modelling; however, the scarcity of water vapour observations at the mesoscale and smaller scales still hampers progress. The origin, pathways and time scales of transport of the large

amounts of moisture necessary for HPSs in the WMed are still open questions. Additionally, our understanding of the distribution, and variability of water vapour in relationship with convection is still far from being complete.

Due to its importance, the characterization of water vapour has been a crucial aspect in the first of the two field campaigns of the Hydrological cycle in the Mediterranean Experiment (HyMeX; Drobinski et al. 2014). The Special Observation Period (SOP1; Ducrocq et al. 2014) provided the unique opportunity of using the synergy of a dense network of observations, available on routinely basis, but homogenized for HyMeX, or especially deployed during the measurement campaign, to investigate the spatio-temporal variability of atmospheric water vapour in the north-WMed area in relationship with convection development. Previous studies analysed the consistency between the different water vapour data sets during the SOP1 (Chazette et al. 2016b). Few studies focused on the assessment of small-scale integrated water vapour (IWV) variability (< 10 km / < 1 day) and/or on the relationship between water vapour and precipitation systems on a larger-scale (> 1000 km / > 1 day; e.g. Van Baelen et al. 2011; Winschall et al. 2012; Chazette et al. 2016a; Lee et al. 2016, 2017).

Using a multispatial scale approach, in this study, we use the synergy of moisture-measuring instruments available during the Intensive Observation Period 12 (IOP 12) to document the evolution and distribution of tropospheric water vapour in relation to the occurrence of HPSs in the north-WMed. Ground-based and airborne observations, as well as space-borne retrievals are combined to obtain a 3-D representation of atmospheric moisture. High-resolution convection permitting numerical weather prediction COSMO model simulations are used to complement the observations and the recent online trajectory module of COSMO helps us calculate online air parcel trajectories in relation with the convection activity in the area. The goal of the present study is to investigate several aspects of the moisture variability-HPSs relationship during IOP12 in the north-WMed, (a) the variability of tropospheric water

vapour and the ability of available observations to properly sample this on different scales, and (b) the role of water vapour as a precursor of heavy precipitation activity in the area. This paper is structured as follows: Section 2 outlines the experimental and modelling setup. Section 3 describes the synoptic situation that dominates over the investigation region between 9 and 14 October, as well as the convection activity and life cycle of the relevant storms in this period. The precipitation distribution, as well as the accompanying lightning activity, is also discussed. In Section 4, the pre-convective environment leading to HPSs in the investigation areas is assessed by detailed joint evaluation of observations and derived calculations. This part is followed by a detailed analysis of the spatial and temporal distribution of atmospheric humidity in Section 5. The transport, horizontal distribution and vertical stratification on different scales over the north-WMed are discussed. Section 6 closes this study with the summary of findings and conclusions.

2. Observational and modelling setup

2.1 Observations

Water vapour-related observations covering the north-WMed area between 9 to 14 October, including the IOP12, are used in this investigation, combining spaceborne and in situ observations from ground-based (Figure 1) and airborne platforms. A short description is provided in the following,

(a) Spaceborne information

- *Rapid Developing Thunderstorm product (RDT)*

The RDT product is used in addition to lightning and precipitation information for a detailed analysis of the life cycle of convective storms during the selected investigation period. This product was developed by a team of specialists from the national

meteorological institutes from Spain (AEMET), France (Météo-France), Sweden (SMHI) and Austria (ZMAG), as part of the Satellite Application Facility to support Nowcasting and Very Short range Forecasting (SAFNWC), hosted by the European Organisation for the Exploitation of Meteorological Satellites (EUMETSAT). It applies an algorithm to combine the Spinning Enhanced Visible and InfraRed Imager (SEVIRI) onboard Meteosat second generation (MSG) and lightning data from ZEUS lightning detection network (operated by the National Observatory of Greece) to identify and track convective systems ranging from single isolated cells to mesoscale convective complexes (NWC SAF, 2014). The visualization tool developed by Météo-France uses colours to mark the development stadium of any identified storm. The available data is presented in an animated form in a 15 min temporal resolution.

- *Moderate Resolution Imaging Spectroradiometer (MODIS)*

In this investigation, MODIS is utilized in order to study the IWV content of the troposphere from the radiance measurements performed by the imaging spectrometers on board the polar-orbiting platforms Terra (crossing the Equator at 1030 LT) and Aqua (crossing the Equator at 1330 LT). IWV is derived by applying an algorithm to IR spectral radiances retrievals obtained with clear sky conditions during either day or night-time (Gao and Kaufman 2003). The result is a highly spatially resolved gridded data set (5x5 km) of IWV, mapping the whole Earth's surface every one or two days. The employed data set for this study is a daily average of both Terra and Aqua observations made available on a grid spacing of $1^{\circ} \times 1^{\circ}$.

- *NOAA CPC Morphing Technique (CMORPH)*

This product provides precipitation estimates during the investigation period in a gridded data set derived from microwave observation instruments placed in different low orbiter satellites. Microwave measurements from the Special Sensor Microwave Imager (SSM/I) aboard the Defence Meteorological Satellite Program satellites (DMSP-13, -14 and -15),

the Advanced Microwave Sounding Unit-B (AMSU-B), on-board the National Oceanic and Atmospheric Administration spacecraft's (NOAA-15, -16, -17 and -18 spacecraft's), the Advanced Microwave Scanning Radiometer-Earth Observing System (AMSR-E) of the Aqua spacecraft and the passive Microwave Imager of the Tropical Rainfall Measuring Mission satellite (TMI-TRMM) are combined by means of the Morphing Technique (Joyce et al. 2004). This procedure makes use of infrared derived motion vectors to propagate the microwave imagers' features to locations where no microwave data were obtained at a specific time (Stampoulis et al. 2013). This renders the technique flexible regarding its applicability to any microwave satellite source. In addition, it offers a wide coverage (60°S to 60°N), and a high temporal and spatial resolution, 30 minutes and 8 km at the Equator. The data set is produced by the Climate Prediction Center (CPC) of the National Weather service (NWS) of the USA and covers the period between 1998 and 2015.

(b) Ground-based information

- *Radiosondes*

Measurements from about 25 radiosounding stations in the HyMeX investigation area (Figure 1) are used for this research effort. On a regular basis, these measurements provide atmospheric profile information at least twice a day (0000 UTC and 1200 UTC). During SOP1, several of these stations either launched additional sondes at 0600 and 1800 UTC and/or conducted high-resolution soundings (meaning here the vertical sampling of the collected data being less than 1 hPa (about 100 vertical levels) in comparison to regular soundings with generally about 20 vertical levels), all in order to provide a more detailed picture of the vertical distribution of atmospheric variables prior to and during the IOPs. Among these, seven stations were newly established for the purposes of the HyMeX SOP1 campaign.

The network of radiosonde stations is additionally used to calculate convection-related parameters as indicators of the atmospheric degree of stability/instability, namely the Convective Available Potential Energy (CAPE; Moncrieff and Miller 1976), the Convective Inhibition (CIN; Colby 1984) and the KO-index (Andersson et al. 1989). The KO-index is estimated based on the equivalent potential temperature at 500, 700, 850 and 1000 hPa (following the recommendations by Bolton 1980), it describes the potential of deep convection to occur as a consequence of large-scale forcing (Andersson et al. 1989; Khodayar et al. 2013). Generally, regions with KO-index < 2 K and large-scale lifting are identified as favourable for deep convection. Parcel theory (50 hPa ML (Mixed Layer) parcel) and virtual temperature correction (Doswell and Rasmussen 1994) are applied to these calculations.

- *Ground-based GPS*

A dense network of Global Positioning System (GPS) stations, which provide IWV information, covering the north-WMed were jointly reprocessed by IGN LAREG (Institut National de l'Information Géographique et Forestière - Laboratoire de Recherche en Géodésie) and e-GEOS S.p.A., ASI/CGS (Agenzia Spaziale Italiana/Centro di Geodesia Spaziale) and made available for the HyMeX scientific community (Bock et al. 2016). One of the highlights of this dataset is its dense and large coverage, provided it was obtained by commonly processing the raw measurements of 25 European, national and regional GPS networks. The post-processing GIPSY/OASIS II v6.2 software was used to process the total delays in the zenith direction (ZTD) and surface level pressure and mean temperature at the stations location were obtained from the AROME model in its west-Mediterranean configuration (AROME-WMED) and ERA-Interim analysis respectively. The dataset is available up to a 5 minute temporal resolution (the nominal sampling

frequency) and also in 1-hourly and 3-hourly averaged data sets. In this study, the 1-hourly averaged product is used.

- *Boundary Layer pressurized balloons (BLBP)*

Lagrangian trajectories of specific humidity, temperature, pressure and horizontal wind can be obtained by means of Boundary Layer Pressurized Balloons (BLPBs) flying at a nearly constant height (Doerenbecher et al. 2016). For HyMeX SOP1, the Centre National d'Études Spatiales (CNES) measured and processed the *BLPB BAMED SOP1* dataset which is made available in 2.5 minute averages of 30-second samples, excluding time windows with less than four measurements available. The different launch dates were selected according to the forecasted conditions which were most propitious to reach targeted heavy precipitation areas during the campaign. Specifically, for IOP12 a total of 4 balloons were launched from the Mahon site ($4^{\circ} 15' - 39^{\circ} 51'$; Balearic Islands); two on the 11 October 2012, at ~ 0200 and 0400 UTC and two on the 14 October 2012, at 0600 and 0800 UTC, respectively. An inter-comparison between water vapour mixing ratio derived from the BLPB trajectories and that obtained from the ground-based water vapour Raman Lidar (WALI) showed a root mean square error of less than 1.3 g kg^{-1} for the SOP1 period over the Balearic Islands (Chazette et al. 2016b). This highlights the good quality of the humidity measurements.

- *Ground-based Raman lidars BASIL (Candillargues) and WALI (Menorca)*

The Raman Lidar BASIL (Di Girolamo *et al.* 2006, 2009a) is very effective in the characterization of atmospheric temperature and water vapour mixing ratio profiles throughout the troposphere, both in daytime and night-time conditions, providing accurate and high time- and space-resolution measurements of these two thermodynamic parameters, with the main goal of characterizing the water vapour inflow in the Gulf of Lion, which is heavily feeding precipitating systems. The system was deployed in an

atmospheric ‘supersite’ located in Candillargues (43°N, 4°E, elevation: 1m) and operated from 5 September to 5 November 2012 (Figure 1). Besides atmospheric temperature and water vapour, BASIL also provides measurements of particle backscatter at 355, 532 and 1064 nm, particle extinction at 355 and 532 nm, and particle depolarization at 355 and 532 nm (Di Girolamo *et al.* 2009b, 2012). During HyMeX-SOP 1, water vapour mixing-ratio measurements were calibrated based on the comparison with the simultaneous radiosondes, with the radiosonde launching facility being located approximately 100 m south-east of the lidar station. A mean calibration coefficient for water vapour mixing ratio measurements was estimated based on approximately 50 comparisons.

The Water Vapour Lidar (WALI) described in Chazette *et al.* (2014) is additionally used to monitor the water vapour mixing in the lower troposphere over the WMed during the period of interest. The lidar was located in La Ciutadella (40°00'00" N and 3°50'20"E) on Menorca Island (Spain, see Figure 1). The measurement protocol is explained in Chazette *et al.* (2016b). During HyMeX SOP1, the absolute deviation between the water vapour mixing ratio profiles from WALI and derived from meteorological balloon soundings launched from Palma de Mallorca was assessed to be less than 0.5 g kg^{-1} for a vertical resolution of 30 m. The maximum range of the zenith-pointing lidar was ~6-7 and 1 km during night-time and daytime, respectively, depending on the atmospheric transmission, mainly limited by the presence of aerosols or/and clouds.

- *Lightning Network*

The European Cooperation for Lightning Detection (EUCLID 2014) is a collaboration of national lightning detection networks with the aim to identify and detect lightning all over Europe. Within our investigation area, 32 sensors from different networks are positioned. All the lightning data are detected by means of electromagnetic sensors, which send raw data to a central analyser. Each sensor detects the electromagnetic signal emitted by the

lightning return stroke. This technology uses GPS satellite signals for time information. For each lightning stroke, the main parameters are recorded, namely, the time of the event, the impact point (latitude and longitude), the current intensity and polarity, and the number of subsequent strokes. This data provides information about the position and even intensity of isolated and organised convective systems.

(c) *Airborne Information*

- *Airborne lidar LEANDRE 2 on board of ATR-42*

The airborne differential absorption lidar (DIAL) LEANDRE 2 was installed on board the ATR-42 aircraft of Service des Avions Français Instrumentés pour la Recherche en Environnement (SAFIRE), which operated from the Montpellier airport during SOP1 (also see Chazette et al. 2016b; Di Girolamo et al. 2016; Lee et al. 2016, among others). Details concerning the design of LEANDRE 2 and the standard DIAL signal processing procedure are given in Bruneau *et al.* (2001a, 2001b). During IOP12, LEANDRE 2 was operated mostly in zenith-pointing mode, except for a small portion of the flight performed over the Gulf of Lion on 11 October when it performed nadir-pointing observations. LEANDRE 2 carries out water vapour mixing ratio measurements with a precision ranging from less than 0.1 g kg^{-1} at 4.5 km above sea level to less than 0.4 g kg^{-1} near the surface for an along-beam resolution of 150 m and accumulation of 100 individual profiles, corresponding to an along-track resolution of approximately 1 km for an ATR-42 flying speed of 100 m s^{-1} . Systematic errors associated with the LEANDRE 2 system are typically not exceeding 0.1 g kg^{-1} (Bruneau et al. 2001b).

- *Do-128*

Do-128 (Corsmeier et al. 2001) flew mainly around and over Corsica from 11 September to 11 October 2012 as a part of the Karlsruhe Institute of Technology (KIT) participation

in HyMeX-SOP 1. It is equipped with instruments (in a nose boom attached on the front) for measuring air temperature, humidity, wind direction and speed, among others.

2.2 COSMO model and online trajectory module

The non-hydrostatic limited-area weather prediction model Consortium for Small-scale Modelling (COSMO), developed by the German Weather Service (DWD, Shättler et al. 2008), is employed in this investigation with horizontal grid spacing of about 7 km and 2.8 km, and 40 and 50 vertical levels, respectively. COSMO-2.8 km explicitly resolves deep convection (Weisman et al. 1997) and shallow convection is parameterized with the help of the reduced Tiedtke scheme (Tiedtke 1989), whereas in COSMO-7 km convection is parameterized with the Tiedtke scheme (Tiedtke 1989). Details about the setup for all physical parameterizations are found in Baldauf et al. (2011). The European Centre for Medium-Range Weather Forecasts (ECMWF) analysis data with a horizontal resolution of about 0.25° is used as initial and boundary conditions for the COSMO-7 km run, while this is used as forcing for the higher resolution COSMO-2.8 km. The COSMO-7 km and 2.8 km model domains extend from about 15°W to 22°E - 25°N to 50°N and 10°W to 20°E - 30°N to 46°N , respectively.

Online Lagrangian trajectories based on grid-scale wind velocities are used to study mesoscale flows in the COSMO model (Miltenberger et al. 2013). The Lagrangian depiction of atmospheric processes largely contributed in the last years to advance our understanding. Lagrangian studies allowed the identification of atmospheric rivers (e.g. Ramos et al. 2015; 2016) and warm conveyor belts (WCB; e.g. Wernli and Davis 1997), the evaporative and moisture water sources for precipitation (e.g. Sodemann et al. 2008; Liberato et al. 2012) or the origin of air parcels feeding convective cells (e.g. Wang and Xue 2012). We use in this study the online Lagrangian trajectories module of COSMO to assess the most likely origin and path of air parcels contributing to the occurrence of HPS during the IOP12 on the WMed.

A great advantage of the online trajectory contrary to any other offline option is the calculation of the trajectory with wind field inputs at every model time step (~ 25 s for the high-resolution simulations, this value shortens with increasing model resolution), whereas offline trajectories are calculated with temporal resolutions from 1 h to 6 h. Because of the forward computation of the online trajectories, the specification of the starting points is not a trivial task. A priori knowledge of the interesting starting regions and times is required. Following Duffourg and Ducrocq (2013) we started the simulation about 4 days before intense convection activity in the north-western Mediterranean to consider the moisture of the low-level feeding flow provided by evaporation over the Mediterranean and the transport from remote sources such as the Atlantic Ocean and/or Africa. The whole simulation period covers the 8 October 2012 to the 16 October 2012. To avoid missing relevant information we start trajectories every 0.5° over the entire investigation domain every 12 h starting 4 days before the event. In total more than 50000 trajectories are calculated. To identify from all estimated trajectories the contributing air parcels to each HPS and their origins the following criteria are applied, (a) all air parcels are started 10 m over the surface to capture moisture uptake regions. We assume that at this height the trajectories start in the boundary layer and trajectories intersection with the terrain is avoided (Miltenberger et al. 2013), (b) air parcel trajectories have to reach at least ~ 7000 m (Wernli 1997), and (c) air parcels have to release at least 5 g kg^{-1} of the specific humidity in a 6-hour interval within the target area (Winschall et al. 2014; Sodemann et al. 2008; James et al. 2004).

3. Meteorological situation

3.1 Large-scale situation

The synoptic situation over the Mediterranean area during the analysed period was generally dominated by a long-wave trough that approached from the west and remained over the Iberian Peninsula for several days, producing favourable conditions for the development of deep moist convection (Figure 2).

On 9 October, the WMed was under the influence of a slowly weakening ridge receding before the appearance of a trough approaching from the eastern Atlantic, which developed from a cut off low that moved across the ocean in the previous days (Figure 2a). It merged with a quickly approaching and elongating trough over the north-western Atlantic in the course of 10 October. On the following day, the trough over the Atlantic moved further south-eastwards (at 0000 UTC its axis stretched along the western Iberian coast). Until late 11 October, a weak low-pressure area moved eastwards along the southern French coast reaching the Gulf of Genoa (Figure 2b). To the west of it, in the upper levels, a well pronounced short-wave trough simultaneously crossed that area, advecting warm and humid air from over the sea. Ahead of it moved an area of strong local lifting (between 20 and 40 hPa in 6 hours). A slight Potential Vorticity (PV) anomaly that accompanied this short-wave trough (not shown) additionally strengthened the already existing instability. During the day, the long-wave trough moved further eastwards so that around 1800 UTC its major axis lay across central France and the eastern coasts of Spain. It was swiftly followed by another secondary trough approaching from the west. On 12 October, this secondary trough was located already on the eastern side of the long-wave trough, crossing over Corsica, central Italy and the Balkan. At 0000 UTC, the weak surface low with accompanying fronts was located over the Gulf of Genoa, in the area of strong convective activity of IOP12. It moved ahead of this secondary trough, slightly weakening on its way, and reached the Balkan around midnight. Its presence was related to strong convective activity as well as an HPS over central and southern Italy, as well as over the Adriatic Sea. Westerly and north-westerly mid-tropospheric winds brought in humid air. The upper level pattern from the previous day remained almost unchanged on 13

October (Figure 2c). The axis of the main long-wave trough moved further east and, by approximately 1800 UTC, stretched along the western Italian coast.

3.2. Convective activity

Between 9 and 13 October 2012, covering the IOP12 period (11 and 12 October), the convective activity in the WMed was very intense. During these days convective activity was observed to move eastwards (Figure 3, Table 1).

Intense convective activity on 10 October was initiated in the early afternoon in the form of several storms over central Spain. One of these, with the longest life span, started at ~ 1345 UTC some 100 km to the west of Madrid and moved in the north-eastward direction. At ~ 2000 UTC, it began to weaken but approximately two hours later it merged with a newly developed storm, whereupon it turned south-east towards the north-eastern Spanish coast from where it continued eastwards until it dissipated over the sea at ~0945 UTC on the following day (marked "A"; Figure 3a). It lasted for about 19.5 h and its anvil grew in this time to almost 39000 km². This storm produced relatively moderate amounts of precipitation, i.e. 50 mm of 24-h accumulated precipitation measured by rain gauges and CMORPH estimates, which occurred only over land. Lightning activity in this area was strong throughout the whole convective period, which lasted till the end of the day (Figure 4a).

The main IOP12 MCS developed in the evening of 11 October over the north-WMed as two initially independent storms. By looking at the 15-min radar reflectivity scan images for this particular analysis (not shown), it could be observed that one of these storms (marked "B1" in Figure 3b) initiated at ~1930 UTC also as two separate convective cells, one over the eastern French Riviera and the other some 30 km to the south of it over the sea. The second storm (marked "B2") resulted from the merging of three smaller cells, which occurred at ~ 2100 over the sea some 100 km to the west of Corsica. Before it happened, numerous single-cell storms developed in the zone between the Balearic Islands and Corsica from approximately

1800 UTC embedded within and moving eastwards with a broad cloud band stretching from southern France to northern Africa. Before those two main storms merged to form a MCS (marked "C"), the northern one lasted for about 7 hours growing up to 37000 km² and the southern one for around 4.5 hours reaching over 23000 km² cloud top surface. At around midnight, both storms merged creating a cluster with the anvil's area of over 130000 km². CMORPH captured the initiation of the main IOP12 MCS as two separate storms (not shown), which produced high and spatially concentrated amounts of precipitation (up to 75 mm in 6 hours); precipitation visibly diminished as the storms merged and propagated eastwards developing in to the main IOP12 MCS existing till the early morning hours of 12 October (Figure 4b). Storm "D" (Figure 3c) started as two cells between Corsica and Italy at around 0200 UTC on 12 October and within the following hour it merged with a storm over central Italy, which developed shortly before midnight on 11 October. In its 8-h-long life it crossed central Italy in south-eastern direction and grew up to 93000 km². This MCS was responsible for the HPS over central Italy on that day. On 12 October, an area of strong precipitation could be observed over the vast region stretching between Corsica, Sicily and the Balkan Peninsula, which was directly connected with the activity of the IOP12 MCSs (Figure 4c). Rain gauges in central Italy measured over 150 mm in about six hours, but about 75 mm over the eastern Spanish coast, Majorca and Sicily. According to CMORPH data, the convective storms over the south-WMed also caused HPSs, during which over 150 mm precipitation could be measured in a period lasting between 6 and 12 hours. The lightning pattern shows that dense lightning activity was present everywhere between southern France and northern Sardinia where the main MCS developed. On 13 October convection occurred over the south-western and central Mediterranean (including northern Africa, southern Italy and the Balkan area); however only over Sicily did a MCS develop and remained active and intense in the second half of the day (marked "M" in Figure 3d) producing about 50 mm accumulated precipitation over land in about 6 hours (Figure 4d), but more than 150 mm rain

over the sea within the same time period (not shown). The lightning data show that the majority of storms over the south-western and southern Mediterranean were merely continuations of convective activity that initiated on the previous day. Most of them were moving in the eastern direction and dissipated in the early afternoon.

4. Daily cycle of convection-related atmospheric conditions

An assessment of the temporal evolution and potential dependencies of convection-related atmospheric conditions on sub-daily scale for those areas where HPS occurrence was registered is shown in Figure 5. The following areas are considered, Area1 covers the north-eastern Iberian Peninsula, Area2 covers Corsica, Area3 is located in central Italy, and Area4 includes Sicily in southern Italy (Figure 1). We are particularly interested in assessing the similarities and differences between the Areal preconditions leading to heavy precipitation. For each region hourly lightning sums using cloud-to-ground lightning data measured by the EUCLID network, as well as the hourly rain rates from CMORPH measurements are considered. We selected one representative radiosounding station for each area (Barcelona for Area1, Figure 5a; KIT-INRA for Area2, Figure 5b; Pratica Di Mare for Area3, Figure 5c; Trapani Birgi for Area4, Figure 5d; positions of the radiosoundings are in Figure 1) to study atmospheric stability and humidity stratification. The radiosounding profile information were used to compute CAPE, KO-index, CIN, as representative of atmospheric instability and inhibition conditions and the mean relative humidity (RH) averaged in the layer between 850 and 700 hPa, as a measurement of the humidity content in the mid-troposphere. Additionally, we included the IWV data from the nearest GPS stations (all located at similar heights; Figure 1), which provided information on the humidity contained in the entire troposphere above the station with 1 hourly temporal resolution.

The general picture confirms a shift of convective activity and moisture maxima from west to east. Lightning activity was well correlated with maxima of precipitation as an indicator of deep convection in agreement with previous observations (Soriano et al. 2001). In all cases the convective activity occurred in periods of maximum IWV (~ 30 to 45 kg m^{-2}). An upper threshold of about 45 kg m^{-2} was identified. Total column atmospheric humidity experiences a notable increase prior to HPSs, mostly in relationship with a change, up to 5 g kg^{-1} , in the lower and mid-levels of the atmosphere (below 700 hPa). The upper atmospheric levels (above ~ 500 hPa; not shown) do not reveal any significant variation. Changes in the lower-troposphere in the pre-convective environment were associated to winds predominantly from the south-southwest and from the west in the layers above. Those stations with higher moisture content in the lower troposphere reveal a lower Lifting Condensation Level (LCL) and a smaller difference between the LCL and the Level of Free Convection (LFC), which is conducive to a more rapid formation of thunderstorms (not shown). For example, an increase of about 4 g kg^{-1} in the lower PBL moisture, registered at southern France (NIM radiosounding station) prior to CI resulted in a decrease of LCL-LFC from ~ 175 hPa on 10 October 1200 UTC to ~ 50 hPa on 11 October 1200 UTC. Furthermore, directly related with the increase of moisture in the lower tropospheric levels an increase in atmospheric instability and a decrease in atmospheric inhibition are also identified prior to HPSs.

In the mid-troposphere the relative humidity was very high, $> 75 \%$, in all deep convection events leading to HPSs. Observations of the convective evolution in Area1, after the main event, show a dry mid-troposphere inhibiting deepening of convective systems despite a further low-tropospheric moisture increase. This supports previous investigations which showed that high amounts of moisture in the mid-troposphere, which could be also due to convection itself, favour deepening of convection and precipitation intensity and its absence constrains its evolution (e.g. Khodayar et al. 2010; Lee et al. 2016). Similar developments are identified in the pre-convective environments of all stations affected by HPSs, which

evidences the crucial role of water vapour horizontal distribution and stratification on the initiation and intensification of convection.

In all cases except Area4, the period of severe convection activity was followed by a humidity decrease (back to values observed at least 24-h prior to CI) resulting from boundary layer winds turning their direction to westerly. The advection of dry air, thus, the moisture decrease was concomitant with an equivalent potential temperature decrease and an increase in atmospheric stability ($CAPE \sim 0 \text{ J kg}^{-1}$; $KO\text{-index} \sim 1 \text{ K}$), not favouring further intensification of convection and suppressing any possibility of CI. In Area4, westerly and south-westerly winds continued advecting moist air over southern Italy after the main convection activity developed in the area, which resulted in a further initiation of deep moist convection in this region on 13 October, primarily affecting the Balkans.

Despite the important commonalities listed above relevant differences are identified regarding the build-up time period of the moisture changes and the resulting vertical stratification. Figure 6 helps us illustrate these findings showing the interdependence between atmospheric instability and atmospheric moisture changes with respect to convective evolution at two of the affected areas/radiosounding stations, Area1/Barcelona (deep convection was observed at about 11 October at 0000 UTC; max prec $\sim 50 \text{ mm day}^{-1}$) and Area4/Trapani Birgi (a MCS developed in the morning and maintained until mid-day on 13 October; max prec $\sim 200 \text{ mm day}^{-1}$). Despite a strong Areal increase of IWV $\sim 20 \text{ kg m}^{-2}$ prior to CI, maximum local precipitation in Area1 did not exceed 50 mm day^{-1} (this is the area registering the lowest precipitation rates). This increase occurred in a period of 36 h and maximum IWV values were up to 45 kg m^{-2} . All atmospheric levels up to 500 hPa were affected, particularly the mid- and low-atmosphere. In this 36 h period, an increase of about 3 g kg^{-1} was observed in the $900 \pm 50 \text{ hPa}$ layer in the last 24 h, the same increase occurred in the $700 \pm 50 \text{ hPa}$ layer but only in the first 12 h. With the increasing moisture the atmosphere became more unstable, as testified by the raising CAPE values to about 1200 J kg^{-1} (decreasing KO-index to -10 K).

Contrary to the observed increase in Area1 the episode of moisture build-up over Area4 was rather sudden (about 10 kg m^{-2} in $\sim 12 \text{ h}$), short-lived (duration of maximum about 12 h) and the maximum IWV did not reach more than $\sim 35 \text{ kg m}^{-2}$, $\sim 10 \text{ kg m}^{-2}$ lower than in Area1. In this area the most intense precipitation event was registered, maximum precipitation of about 200 mm in 6 hours was measured around 1200 UTC on 13 October. In contrast to the other regions considered, a rapid and significant moisture increase of about 5 g kg^{-1} in 6 h characterizes the low-troposphere (in Area1 the same maximum in the lower-PBL was reached after a 24 h period), while a weaker change occurs in the mid-troposphere. This resulted in very high CAPE values of about 2000 J kg^{-1} , KO-index $\sim -14 \text{ K}$, in a period where no CIN constrains deep convection in the area.

A similar situation is observed in Area2 and Area3, in which the IWV increase was sudden and rather quick, $\sim 12 \text{ h}$, and the atmosphere did not remain this moist for more than $\sim 12 \text{ h}$ and did not exceed 35 kg m^{-2} . In Area2, between the surface and 700 hPa a specific humidity increase over 3 g kg^{-1} is registered. Moderate CAPE $\sim 500 \text{ J kg}^{-1}$, and KO-index $\sim -9 \text{ K}$ suggest that deep convection is possible in the area only under strong large-scale forcing. In Area3, the specific humidity increased by some 3.5 g kg^{-1} on average between 750 and 600 hPa, whereas an increase of about 2 g kg^{-1} is identified below 900 hPa resulting in a sudden increase of CAPE to $\sim 800 \text{ J kg}^{-1}$. The combination of these changes with the lack of atmospheric inhibition, CIN $\sim 0 \text{ J kg}^{-1}$, favoured deep convection and intense precipitation in the area. More than 150 mm in 6 h were measured in the area.

5. Moisture transport and distribution over the north Western Mediterranean

To complement the information provided by the single observations regarding the evolution of moisture with respect to convective activity in the selected subdomains, a combination of MODIS and GPS-derived IWV (Figure 7) and observations from the two ground-based water

vapour Raman Lidars, WALI at Menorca (Balearic Islands) and BASIL at Candillargues (Southern France; Figure 10) and from the BLPBs (Figure 11a) and the airborne water vapour lidar (Figure 11b,c,d) are investigated. These measurements should complement each other and their joint evaluation is expected to provide an improved representation of atmospheric moisture variability and its implication for convective activity on different spatiotemporal scales.

The combination of MODIS and GPS-derived IWV allows the reconstruction of the spatial distribution of tropospheric water vapour over a large area, being a well-known limitation of observational networks such as the GPS (Khodayar et al. 2016b). To jointly evaluate both data sets, comparisons have been performed at the location of each GPS-station. Maximum differences of about 2 kg m^{-2} have been found, which could be related with cloud contamination in the MODIS IR data (dry bias) and with the time sampling differences. No bias correction has been applied in this case. This information is combined with simulated high-resolution, 7 km and 2.8 km, COSMO winds at different levels (500, 700, 850, 950 hPa and 10 m), in order to assess the most likely transport path of the atmospheric moisture during IOP12. Furthermore, the computation of the COSMO online Lagrangian trajectories helped us to further assess the trajectories that air parcels mostly contributing to the HPS followed serving as a qualitative indicator of the most likely transport pathway (Figure 8a) and origin (Figure 8b) of moisture.

On the 9 October 2012, MODIS-derived IWV shows two hot-spots with IWV values reaching about 50 kg m^{-2} , over the Atlantic – between Portugal and north-Africa – and east of Tunisia (Figure 7a). Following the south-westerly transport of humid air from the Atlantic towards the centre and north of the Iberian Peninsula a gradual humidity surge of about 10 kg m^{-2} could be observed throughout the day, from about 25 to 35 kg m^{-2} . On 10 October, moisture

advection continues over the Iberian Peninsula and the moisture amount over the already relatively humid Mediterranean ($30 - 35 \text{ kg m}^{-2}$) rose up to 45 kg m^{-2} forming a humid zone along the eastern Spanish coast bending eastward across the Balearic Sea up to Sardinia (Figure 7b). Instability began to increase over the Iberian Peninsula, reaching CAPE values of ca 1000 J kg^{-1} and KO-index of about -15 K over Barcelona (Figure 9a). The first storms initiated over this area (Figure 3a) in the presence of some moderate CIN over Barcelona (ca 80 J kg^{-1}) and a relatively strong one (250 J kg^{-1}) over Zaragoza, about 250 km apart. Several orographically induced convergence lines formed over central and eastern Spain on that day, some as early as 12 h prior to the formation of the first storms in the region. The position of these convergence lines did not change much during the day, but winds became stronger as the day progressed (a change from 1 to about 8 m s^{-1} was measured). This low-level wind convergence in addition to the presence of large scale lifting of about 20 hPa h^{-1} acted as triggering mechanisms in the area. KO-index in the order of -15 to -20 K and high CAPE ($\sim 900 \text{ J kg}^{-1}$) in combination with no CIN occur also over Corsica, in agreement with high moisture values observed e.g. at the INRA radiosounding station (Figure 5b). However, no convection developed in this area due to the absence of a triggering mechanism, contrary to the previous situation on the north-eastern Spain.

The eastward transport of moist air continued on 11 October (Figure 7c). This eastward gradual moisture increase was strongly correlated (spatially and temporarily) with the moist air advection associated with the surface low accompanied by the shortwave trough aloft (Figure 2). Accompanying the strong increase of moisture along the southern French coast and Majorca, then over Corsica (reaching about 40 kg m^{-2} from a value of $\sim 20 \text{ kg m}^{-2}$ 24 h before), CAPE levels increased (between 1000 and 1750 J kg^{-1} ; Figure 9b) particularly between the Gulf of Lion and northern Algeria. CIN levels in that same region were the highest in the south (up to 150 J kg^{-1} over Dar El Beïda) and the lowest in the north (between 0 and 10 J kg^{-1} over southern France) where deep convection initiated, which led to the

development of the main IOP12 MCS (Figures 3 and 4). Also in this case, a convergence zone could be identified from the near-surface wind and buoy observations (not shown) prior to CI, also captured by COSMO 2.8 km. The convergence line southeast of the Gulf of Lion was already present at about 1200 UTC because of the merging of north-easterly and south-westerly winds, which additionally advected moist air from over the sea. The 500 hPa level was a region of strong air ascent (between 20 hPa h^{-1} over southern France and almost 40 hPa h^{-1} over the sea) associated with the short-wave trough. In agreement with these observations and complementing this information, the computation of the COSMO online Lagrangian trajectories showed four main regions from where air parcels contributed to the formation of the HPSs: a) the eastern Atlantic Ocean, b) the land over the Iberian Peninsula, c) the north-western Mediterranean, and d) the north-eastern Africa region. Regions a, b and c mainly contributed to the formation of the HPSs over central and eastern Spain on 10 October, whereas regions c and d play this role for the main IOP12 HPS on 11 and 12 October. Different time scales ranging from days to hours are needed for the air parcels originating at these regions to reach the target areas. Remote regions such as the Atlantic Ocean and Africa require about 3-4 days whereas closer regions such as the Mediterranean itself need few hours to a day to reach their destination.

The ground-based water vapour Raman Lidars WALI and BASIL (Figure 10), the BLPBs (Figure 11a) and the airborne lidar LEANDRE 2 (Figure 11b1, 11b2, 11b3) additionally provided some valuable insight into the atmospheric moisture conditions directly over the region where the IOP12 MCS initiated. The south to north moisture gradient and the increasing moistening of the atmosphere preceding deep convection, which determined CI location in the area, was well captured with high resolution. At Menorca, WALI (Figure 10a) reveals a very moist low PBL, with specific humidity values up to about 15 g kg^{-1} and reaching up to ca 1.5 km, from 9 October until early morning on 12 October. At 0000 UTC on 12 October, deep moist updrafts are seen, probably in relationship with strong updrafts

transporting moist air from the lower levels. This is in contrast with the dry atmosphere in southern France as evidenced by the BASIL lidar observations for the period 10 to 12 October (Figure 10b). Maximum values of water vapour up to 10 g kg^{-1} are seen reaching about 1 km, in the period between 11 October at 1200 UTC and 12 October at 0000 UTC. The BLPBs captured a high level of variability in the area between the Balearic Islands and Corsica on 11 October. In the initial part of their eastward trajectories, both balloons measured moisture amounts of roughly 10 g kg^{-1} . This changed as they both turned northwards where, in both cases, specific humidity levels increased to about 15 g kg^{-1} ($\sim 6\text{-}10 \text{ g kg}^{-1}$ moister than observations on the same region on the 14 October). On this day, a short Do-128 flight conducted from 0700 till 1100 UTC over the sea along the north-eastern Corsican coast clearly evidenced that the lower PBL ($\sim 200 \text{ m amsl}$) in this region was significantly drier, $< 5 \text{ g kg}^{-1}$, than the western coast.

In agreement with this, the LEANDRE lidar on board of the ATR-42 (between ca 0600 and 1000 UTC on 11 October over the eastern Gulf of Lion, upstream of convective systems developing over this region at about 1930 UTC) showed a very moist PBL, reaching up to ca 1.5 km, with specific humidity levels between about 9 and 15 g kg^{-1} (Figure 11b1). On the contrary, on 12 and 14 October (as part of IOP13) in the same area, a shallow PBL reaching up to 0.5 km was observed with specific humidity values between 6 and 11 g kg^{-1} in this layer (Figures 11b2 and 11b3). Figure 7d shows that after this period moisture content decreases over the Iberian Peninsula, France and Corsica and Sardinia Islands (by 10 to 20 kg m^{-2} on average) in agreement with the south-eastward progress of notably drier air. In all those regions, it put an end to severe convection.

A change to southerly winds in the lower-troposphere over eastern-Africa and over the sea east of Tunisia, starting at about 1800 UTC on the 11 October, is responsible for the transport of the moist air mass over the sea towards central Italy (an IWV increase of about 15 kg m^{-2} in less than 24 hours is registered). These changes were closely correlated with the drop in

instability (CAPE and KO-index) in the western part of the investigation area, and a gradual increase everywhere in the east, beginning over Corsica and moving southeast towards southern Italy (Figure 9c). Under these conditions convection activity over central Italy started entering in its dissipation stage at around 1600 UTC on 12 October. Preceded by a IWV increase in the area of Sicily, from around 30 kg m^{-2} measured at 1800 UTC on 12 October to around 40 kg m^{-2} at 0700 UTC on 13 October, and accompanying CAPE values in the range $1500\text{-}2000 \text{ J kg}^{-1}$, KO-index close to -20 K and almost no CIN, the severe MCS (Figures 3 and 4) producing another HPS, with precipitation sums up to 200 mm in 6 hours, occurred in southern Sicily. Several convergence lines were also present over western Italy and the northern Tyrrhenian Sea prior to the onset convection in the night between 11 and 12 October. In this case, these formed only some 3 h prior to convective CI. Their effect was strengthened by a shortwave trough aloft and the orography of the area which played an important role in this case. The front approaching from the northwest forced the moist air ahead of it ($\text{IWV} \sim 40 \text{ kg m}^{-2}$) to rise over the western slopes of the mountain ranges stretching along the Apennine Peninsula. On 13 October (Figure 7e), dry air masses continued to flow in from the north-western direction over Spain, France, and north- and central Italy. By the end of the day the IWV levels dropped to values as low as $10 - 15 \text{ kg m}^{-2}$. The most humid air was concentrated over the south-eastern part of our investigation area (Algeria and Tunisia to the south), and over the Tyrrhenian Sea and to the south and west of Sicily, where till noon moisture levels rose up to 40 kg m^{-2} . In this area, a low-level wind convergence zone could be identified resulting from the merging of southerly winds transporting moisture from the sea east of Tunisia, and northerly winds transporting moisture from the Mediterranean area between Sardinia and central Italy. This convergence zone favoured the concentration of the convective activity around Sicily, especially west of it over the sea. Everywhere the humidity started to decrease in the early evening and remained low in the following days. Figure 9d shows that instability decreased in almost the whole region and

CIN increased by 50 to 70 J kg⁻¹ with respect to the values measured 24 hours earlier. Convection was still active over the Tyrrhenian Sea and Apennine Peninsula in the afternoon and evening of 13 October, but it was no longer as intensive as on the previous day.

6. Conclusions

The investigation of the spatio-temporal evolution of atmospheric moisture variability contributing to the HPS over the WMed region is an open question whose progress is generally hampered by the lack of water vapour observations, thus mostly restricted to modelling studies. This study profits from the rare opportunity to gather a diverse set of observational data sets providing a representation of atmospheric moisture across spatial and temporal scales in the framework of HyMeX. This helped us demonstrating that the sampling of water vapour spatial inhomogeneities on different scales is crucial for the understanding of the timing and location of deep convection. With this purpose, we use three types of observations, passive remote sensing water vapour observations such as MODIS, ground-based in-situ measurements such as radiosounding profile information, BLPB, ground-based water vapour Raman lidars and GPS-derived IWV, as well as airborne water vapour DIAL measurements. We combine this information with high-resolution COSMO model simulations to provide insight into the origin and pathways of air parcels contributing to the occurrence of the MCSs and their triggering mechanisms. Regarding this last point, the identification of low-level wind convergence lines prior to each deep convection episode in the area turned out to be crucial for the initiation and location of convection in the area, which is in agreement with previous investigations in different mid-latitude regions (e.g. Khodayar et al. 2013).

Four areas of intense deep convection activity affect the investigation area during IOP12. Convective activity starts in north-east Spain (Area1) moving eastward toward Corsica (Area2), where intensification is observed and finally affecting central (Area3) and southern

Italy (Area4). Italy was the most affected area, with intense precipitation being registered, ~ 150-200 mm/6 h, while precipitation rates in the range 50 to 100 mm in 24 h were recorded in the other affected areas.

The main findings of this study are summarized below,

- The high spatial and temporal coverage of GPS-IWV observations allowed to adequately sampling the west-to-east moisture transport within the north-WMed. All convective episodes leading to HPS occurred in environments with IWV values between 30 and 45 kg m⁻², being these upper threshold values common in the region for the autumn period of 2012 (e.g. Khodayar et al 2016a).
- Large moisture changes, up to 20 kg m⁻², were identified prior to each convective episode leading to HPS. More intense events were not related to the situations in which higher IWV is reached, but rather the build-up time and vertical distribution of these increases were found to be crucial for the evolution and intensification of the HPS, thus on the severity of the event.
- The most intense events reveal a rapid, 6-12 h, IWV increase in the order of 10 kg m⁻² (Area2, Area3 and Area4), whereas less intense events show a larger increase, ~ 20 kg m⁻² but in a longer time period 24h to 36 h (Area1).
- Total column moisture changes were mainly related to differences in the lower and mid-troposphere. Almost no change in the atmospheric moisture distribution was observed at ~ 500 hPa or above. The mid-atmosphere, ~ 850 to 700 hPa, remained very moist during the pre- and convective periods, with RH values in excess of 75 %, favouring deep convection development. In the lower-troposphere, changes up to 5 g kg⁻¹ are observed.
- The atmospheric stability conditions were as expected largely affected by these changes. The larger/faster the increase of the water vapour content in the low- and

mid-troposphere, the stronger the impact on the atmospheric stability conditions and the strength of convection. Large-sudden increases in CAPE are identified preceding explosive convection yielding high precipitation amounts in a few hours.

- A decrease of the LCL and a reduction of LCL-LFC are identified in those situations following an increase of moisture in the lower-troposphere. This suggests that moist air parcels become more easily buoyant, thus favouring initiation of deep convection and the rapid formation of deep thunderstorms.
- Moister and deeper boundary layers with updraughts reaching up to 2 km are identified in those pre-convective environments leading to HPS, whereas dry, shallow boundary layers are found everywhere else with updraughts not higher than about 1 km.
- Spatial moisture inhomogeneities in the lower PBL, up to 4 g kg^{-1} in less of 100 km, have been shown to determine the location of CI over the sea.
- Particularly for this IOP12, the more intense HPS is seen to receive air parcels, hence moisture contributions simultaneously from different sources resulting in a large-sudden increase of moisture in the lower atmosphere leading to explosive HPSs, as previously discussed. Whereas in the less intense events advection from a particular direction is seen to control moisture changes in the lower and mainly mid-troposphere probably in relation to synoptic conditions dominating the dynamics of the atmosphere. After the occurrence of heavy precipitation, a strong decrease of atmospheric moisture content is seen with the same or larger magnitude of the previous increase.

We can conclude that the combined analysis of the available observational data sets provides on different scales adequate information about atmospheric moisture variability relevant to HPS occurrence. The synergetic analysis of the measurements helped us understanding the

mechanisms and pre-convective conditions leading to deep convection in the area. Limitations on the use of single instrumentations are pointed out in this study. The development of a lidar network to measure water vapour could be of great help in the understanding and forecast of extreme events. The sampling of the interplay between the moisture evolution on different scales, from the large- to the smaller scale, as well as the lapse rate in which this occurs is crucial to improve our understanding of HPSs. Additionally, this study demonstrates that the misrepresentation of this variability in time and space should be carefully evaluated in model simulations as a crucial factor responsible for wrong CI and precipitation simulations. This study focuses on a complex single IOP; therefore, it would be of interest to extend the investigation to a large number of events, including other types of convective situations. Although the relevance of the vertical distribution of moisture and related changes for the occurrence of HPSs was already pointed out in the region in Khodayar et al. (2016c), the relationship with the severity of the event and the build-up time has not been previously discussed. Therefore, further analysis regarding these characteristics will be necessary to assess the generality of our results.

Acknowledgements

This work is a contribution to the HyMeX program supported by CNRS MISTRALS, ANR IODA-MED Grant ANR-11-BS56-0005, ANR MUSIC Grant ANR-14-CEO1-014 and ANR REMEMBER Grant ANR-12-SENV-001. The authors thank the HyMeX database teams (ESPRI/IPSL and SEDOO/Observatoire Midi-Pyrénées) for their help in accessing the data, as well as all SOP1 field teams who performed measurements during this time. We further acknowledge U. Corsmeier, A. Wieser and the whole crew of the Do-128 and ATR-42 for performing and facilitating aircraft measurements. Airborne data was obtained using the ATR-42 Environment Research Aircraft operated and managed by Service des Avions Français Instrumentés pour la Recherche en Environnement (SAFIRE), which is a joint entity of CNRS, Météo-France & CNES. The SAFIRE staff is thanked for their support during the SOP1. The authors are grateful to D. Bruneau, P. Genau, C. Merlet, T. Deleporte, S. Bastin, C. Kocha, C. Lavaysse and R. Meynadier (LATMOS) as well as F. Blouzon and A. Abchiche (DT/INSU) for operating the LEANDRE 2 system aboard the ATR-42 during the HyMeX-SOP1. Finally, we thank EUCLID (EUropean Cooperation for LIghtning Detection) for providing the lightning data and A. Doerenbecher and all teams responsible for the BLPB measurements. The first author's research is supported by the Bundesministerium für Bildung und Forschung (BMBF).

References

Andersson, T., Andersson, M., Jacobsson, C., Nilsson, S. (1989). Thermodynamic indices for forecasting thunderstorms in southern Sweden. *Meteorol Mag* 118(1404), 141–146.

Baldauf, M., Seifert, A., Förstner, J., Majewski, D., Raschendorfer, M., and Reinhardt, T., (2011). Operational Convective-Scale Numerical Weather Prediction with the COSMO Model: Description and Sensitivities. *Mon. Wea. Rev.*, 139(12), 3887–3905. doi.org/10.1175/MWR-D-10-05013.1.

Bevis, M., Businger, S., Herring, T. A., Rocken, C., Anthes, R. A., and Ware, R. H. (1992). GPS meteorology: Remote sensing of atmospheric water vapor using the global positioning system, *J. Geophys. Res.*, 97(D14), 15787–15801. doi:10.1029/92JD01517.

Bock, O., Bosser, P., Pacione, R., Nuret, M., Fourrié, N. and Parracho, A. (2016). A high-quality reprocessed ground-based GPS dataset for atmospheric process studies, radiosonde and model evaluation, and reanalysis of HyMeX Special Observing Period, *QJRMS*, 142(S1), 56-71. doi: 10.1002/qj.2701.

Bolton, D. (1980). The Computation of Equivalent Potential Temperature. *Mon Weather Rev*, 108(7), 1046–1053. doi: 10.1175/1520-0493(1980)108<1046:TCOEPT>2.0.CO;2.

Bony, S., R. Colman, V.M. Kattsov, R.P. Allan, C.S. Bretherton, J. Dufresne, A. Hall, S. Hallegatte, M.M. Holland, W. Ingram, D.A. Randall, B.J. Soden, G. Tselioudis, and M.J.

Webb (2006). How Well Do We Understand and Evaluate Climate Change Feedback Processes?. *J. Climate*, 19, 3445–3482, <https://doi.org/10.1175/JCLI3819.1>

Bruneau, D., Quaglia, P., Flamant, C., Meissonnier, M., Pelon, J. (2001a). Airborne lidar LEANDRE II for water-vapor profiling in the troposphere. I: System description. *Appl. Opt.*, 40(21), 3450–3461.

Bruneau, D., Quaglia, P., Flamant, C., Pelon, J. (2001b). Airborne lidar LEANDRE II for water-vapor profiling in the troposphere. II: First results. *Appl. Opt.*, 40(21), 3462–3475.

Chazette, P., Marnas, F., and Totems, J. (2014). The mobile Water vapor Aerosol Raman Lidar and its implication in the framework of the HyMeX and ChArMEx programs: application to a dust transport process. *Atmos. Meas. Tech.*, 7(6), 1629–1647. doi:10.5194/amt-7-1629-2014.

Chazette P., Flamant, C., Raut, J.-C., Totems J., and Shang, X., (2016a). Tropical moisture enriched storm tracks over the Mediterranean and their link with intense rainfall in the Cevennes-Vivarais area during HyMeX. *QJRMS*, 142(S1), 320-334.

Chazette P., Flamant, C., Shang, X., Totems, J., Raut, J.-C., Doerenbecher, A., Ducrocq, V., Fourrié, N., Bock, O., Dorenbecher, A., and Cloché, S. (2016b). Multi-instrument and multi-model assessment of atmospheric moisture variability over the Western Mediterranean during HyMeX. *QJRMS*, 142(S1), 7-22.

Colby, F.P., (1984). Convective inhibition as a predictor of convection during AVE-SESAME II. *Mon. Wea. Rev.* 112(11), 2239–2252.

Corsmeier, U.; Hankers, R.; Wieser, A. (2001). Airborne turbulence measurements in the lower troposphere onboard the research aircraft Dornier 128-6, D-IBUF. *Meteorol. Zeit.*, 10, 4, 315-329. DOI: 10.1127/0941-2948/2001/0010-0315

Crook, N. A., (1996). Sensitivity of moist convection forced by boundary layer processes to low-level thermodynamic fields. *Mon. Wea. Rev.*, 124(8), 1768–1785.

Di Girolamo, P., Behrendt, A., and Wulfmeyer, V. (2006). Spaceborne profiling of atmospheric temperature and particle extinction with pure rotational Raman Lidar and of relative humidity in combination with differential absorption Lidar: performance simulations. *Appl. Opt.*, 45(11), 2474-2494. doi: 10.1364/AO.45.002474.

Di Girolamo, P., Summa, D., Ferretti, R. (2009a). Multiparameter Raman Lidar Measurements for the Characterization of a Dry Stratospheric Intrusion Event. *J. Atm. Ocean. Tech.*, 26(9), 1742-1762, doi: 10.1175/2009JTECHA1253.1.

Di Girolamo, P., Summa, D., Lin, R. F., Maestri, T., Rizzi, R., Masiello, G. (2009b). UV Raman lidar measurements of relative humidity for the characterization of cirrus cloud microphysical properties. *Atmos. Chem. Phys.*, 9(22), 8799-8811. doi:10.5194/acp-9-8799-2009.

Di Girolamo, P., Summa, D., Bhawar, R., Di Iorio, T., Cacciani, M., Veselovskii, I., Dubovik, O., Kolgotin, A. (2012). Raman lidar observations of a Saharan dust outbreak event: Characterization of the dust optical properties and determination of particle size and microphysical parameters. *Atmos. Envir.*, 50, 66-78. doi: 10.1016/j.atmosenv.2011.12.0612.

Di Girolamo, P., Flamant, C., Cacciani, M., Richard, E., Ducrocq, V., Summa, D., Stelitano, D., Fourrié, N., and Saïd, F. (2016). Observation of low-level wind reversals in the Gulf of Lion area and their impact on the water vapour variability. *QJRMS*, 142(S1), 153-172. doi: 10.1002/qj.2767.

Doerenbecher, A., Basdevant, C., Drobinski, P., Bernard, F., Durand, P., Cocquerez, P., Verdier, N., and Vargas, A. (2016). Low atmosphere drifting balloons: Platforms for environment monitoring and forecast improvement, *Bull. Amer. Meteorol. Soc.*, 97(9), 1583–1599. doi:10.1175/BAMS-D-14-00182.1.

Doswell, C.A. III, and Rasmussen, E.N. (1994). The effect of neglecting the virtual temperature correction on CAPE calculations. *Wea. Forecasting*, 9(4), 619-623.

Doswell C. A. III, Brooks, H. E., and Maddox, R. A. (1996). Flash Flood Forecasting: An Ingredients-Based Methodology. *Wea. Forecasting*, 11(4), 560–581. doi: [http://dx.doi.org/10.1175/1520-0434\(1996\)011<0560:FFFAIB>2.0.CO;2](http://dx.doi.org/10.1175/1520-0434(1996)011<0560:FFFAIB>2.0.CO;2).

Drobinski P., Ducrocq, V., Alpert, P., Anagnostou, E., Béranger, K., Borga, M., Braud, I., Chanzy, A., Davolio, S., Delrieu, G., Estournel, C., Filali Boubrahmi, N., Font, J., Grubišić, V., Gualdi, S., Homar, V., Ivančan-Picek, B., Kottmeier, C., Kotroni, V., Lagouvardos, K., Lionello, P., Llasat, M. C., Ludwig, W., Lutoff, C., Mariotti, A., Richard, E., Romero, R., Rotunno, R., Roussot, O., Ruin, I., Somot, S., Taupier-Letage, I., Tintore, J., Uijlenhoet, R. and Wernli, H., (2014). HyMeX: A 10-year multidisciplinary program on the Mediterranean water cycle. *Bull. Amer. Meteor. Soc.*, 95(7), 1063–1082. doi: <http://dx.doi.org/10.1175/BAMS-D-12-00242.1>.

Ducrocq, V., Braud, I., Davolio, S., Ferretti, R., Flamant, C., Jansa, A., Kalthoff, N., Richard, E., Taupier-Letage, I., Ayrat, P., Belamari, S., Berne, A., Borga, M., Boudevillain, B., Bock,

O., Boichard, J., Bouin, M., Bousquet, O., Bouvier, C., Chiggiato, J., Cimini, D., Corsmeier, U., Coppola, L., Cocquerez, C., Defer, E., Delanoë, J., Di Girolamo, P., Doerenbecher, A., Drobinski, P., Dufournet, Y., Fourrié, N., Gourley, J. J., Labatut, L., Lambert, D., Le Coz, J., Marzano, F. S., Molinié, G., Montani, A., Nord, G., Nuret, M., Ramage, K., Rison, W., Roussot, O., Said, F., Schwarzenboeck, A., Testor, P., Van Baelen, J., Vincendon, B., Aran, M., and Tamayo, J. (2014). HyMeX-SOP1: The field campaign dedicated to heavy precipitation and flash flooding in the Northwestern Mediterranean. *Bull. Amer. Meteor. Soc.*, 95(7), 1083–1100. doi: <http://dx.doi.org/10.1175/BAMS-D-12-00244.1>.

Duffourg, F., and Ducrocq, V. (2013). Assessment of the water supply to Mediterranean heavy precipitation: a method based on finely designed water budgets. *Atmos. Sci. Lett.*, 14(3), 133–138. DOI: 10.1002/asl2.429.

EUCLID (2014). European Cooperation for Lightning Detection. URL www.euclid.org, last accessed on: 9.10.2014

Gao, B., and Kaufman, Y. (2003). Water vapor retrievals using Moderate Resolution ImagingSpectroradiometer (MODIS) near-infrared channels. *Journal of Geophysical Research*, 108(D13).

James, P., A. Stohl, N. Spichtinger, S. Eckhardt, and C. Forster (2004), Climatological aspects of the extreme European rainfall of August 2002 and a trajectory method for estimating the associated evaporative source regions, *Nat. Hazards Earth Syst. Sci.*, 4, 733–746.

Joyce, R., Janowiak, J. E., Arkin, P. A. and Xie, P. (2004). CMORPH: A Method that Produces Global Precipitation Estimates from Passive Microwave and Infrared Data at High Spatial and Temporal Resolution. *Journal of Hydrometeorology*, 5(3), 487-503.

Khodayar, S., Kalthoff, N., Wickert, J., Corsmeier, U., Morcrette, C. J., Kottmeier, C. (2010). The increase of spatial data resolution for the detection of the initiation of convection. A case study from CSIP. *Meteorol. Z.*, 19(2), 179-198.

Khodayar, S., Kalthoff, N., Wickert, J., Kottmeier, C., Dorninger, M.,(2013). High resolution representation of the mechanisms responsible for the initiation of isolated thunderstorms over flat and complex terrains: Analysis of CSIP and COPS cases. *Meteorol. Atmos. Phys.*, 119(3-4), 109-124.

Khodayar, S., Kalthoff, N., Kottmeier, C. (2016a). Atmospheric Conditions Associated with Heavy Precipitation Events in Comparison to Seasonal Means in the Western Mediterranean Region. *Climate Dyn.* 1-17. doi: 10.1007/s00382-016-3058-y

Khodayar, S., Raff, F., Kalthoff, N. and Bock, O. (2016b), Diagnostic study of a high-precipitation event in the Western Mediterranean: adequacy of current operational networks. *Q.J.R. Meteorol. Soc.*, 142: 72–85. doi:10.1002/qj.2600

Khodayar, S. , Fossier, G. , Berthou, S. , Davolio, S. , Drobinski, P. , Ducrocq, V. , Ferretti, R. , Nuret, M. , Pichelli, E. , Richard, E. and Bock, O. (2016c), A seamless weather–climate multi-model intercomparison on the representation of a high impact weather event in the western Mediterranean: HyMeX IOP12. *Q.J.R. Meteorol. Soc.*, 142: 433-452. doi:[10.1002/qj.2700](https://doi.org/10.1002/qj.2700)

Lascaux, F., Richard, E., Keil, C. and Bock, O. (2004). Impact of the MAP reanalysis on the numerical simulation of the MAP IOP2a convective system, ICAM 2003. *Meteorol. Z.*, 13(1), 49–54.

Lee, K.-O., Flamant, C., Ducrocq, V., Duffourg, F., Fourrié, N. and Davolio, S. (2016). Convective initiation and maintenance processes of two back-building mesoscale convective systems leading to heavy precipitation events in Southern Italy during HyMeX IOP 13. *QJRMS*, 142(700), 2623-2635.

Lee, K.-O., C. Flamant, V. Ducrocq, F. Duffourg, N. Fourrié, J. Delanoë and J. Bech, (2017) Initiation and development of a mesoscale convective system in the Ebro River Valley and related heavy precipitation over north-eastern Spain during HyMeX IOP 15a, *Q. J. Roy. Meteorol. Soc.*, 143, 942-956, doi: 10.1002/qj.2978

Liberato, M. L. R., Ramos, A. M., Trigo, R. M., Trigo, I. F., Durán-Quesada, A. M., Nieto, R., Gimeno, L., (2012) Moisture Sources and Large-Scale Dynamics Associated With a Flash Flood Event, *Lagrangian Modeling of the Atmosphere. Geophysical Monograph Series 200*, 111-126 DOI: 10.1029/2012GM001244

Miltenberger, A. K., Pfahl, S., and Wernli, H. (2013). An online trajectory module (version 1.0) for the nonhydrostatic numerical weather prediction model COSMO. *Geosci. Model Dev.*, 6(6), 1989-2004. <https://doi.org/10.5194/gmd-6-1989-2013>.

Moncrieff, M.W, Miller, M.J, (1976). The dynamics and simulation of tropical cumulonimbus and squall lines. *QJRMS*, 102(432), 373–394.

Nuissier, O., Ducrocq, V., Ricard, D., Lebeaupin, C., and Anquetin, S. (2008). A numerical study of three catastrophic precipitating events over southern France, I: Numerical framework and synoptic ingredients. *QJRMS*, 134(630), 111–130.

Nuissier, O., Joly, B., Joly, A., Ducrocq, V., (2011). A statistical downscaling to identify the Large Scale Circulation patterns associated with Heavy Precipitation Events over southern France. *QJRMS*, 137(660), 1812-1827.

NWC SAF (2014). SAFNWC General information. URL <http://www.nwcsaf.org/HD/MainNS.jsp>, last accessed on: 9.10.2014.

Ramos, A.M., Trigo, R.M., Liberato, M.L.R., Tome, R., (2015) Daily Precipitation Extreme Events in the Iberian Peninsula and Its Association with Atmospheric Rivers, *Journal of Hydrometeorology*, 16, 579-597 DOI: 10.1175/JHM-D-14-0103.1

Ramos, A. M., Nieto, R., Tomé, R., Gimeno, L., Trigo, R.M., Liberato, M.L.R., Lavers, D.A., (2016) Atmospheric rivers moisture sources from a Lagrangian perspective, *Earth Syst. Dynam.*, 7, 371-384 DOI: 10.5194/esd-7-371-2016

Riosalido, R. (1990). Characterization of mesoscale convective systems by satellite pictures during PREVIMET-89. Segundo Simposio Nacional de Predicción Madrid, Instituto Nacional de Meteorología, 135–148.

Röhner, L., Nerding, K.-U., and Corsmeier, U., (2016). Diagnostic study of a HyMeX heavy precipitation events over Spain by investigation of moisture trajectories. *QJRMS*, 142(S1), 287-297. DOI: 10.1002/qj.2825.

Schättler, U., Doms, G., and Schraff, C. (2008), A Description of the Nonhydrostatic Regional COSMO-Model, Part VII: User's Guide, 135 pp., *Dtsch. Wetterdienst*, Offenbach, Germany.

Sherwood, S. C., Roca, R., Weckwerth, T. M., and Andronova, N. G. (2010). Tropospheric water vapor convection and climate. *Rev. Geophys.*, 48(2). doi:10.1029/2009RG000301.

Sodemann, H., Schwierz, C., and Wernli, H. (2008). Interannual variability of Greenland winter precipitation sources: Lagrangian moisture diagnostic and North Atlantic Oscillation influence. *J. Geophys. Res.*, 113(D3), D03107. doi:10.1029/2007JD008503.

Soriano, L.R., F. de Pablo, and E.G. Díez, (2001). Relationship between Convective Precipitation and Cloud-to-Ground Lightning in the Iberian Peninsula. *Mon. Wea. Rev.*, 129, 2998–3003, [https://doi.org/10.1175/1520-0493\(2001\)129<2998:RBCPAC>2.0.CO;2](https://doi.org/10.1175/1520-0493(2001)129<2998:RBCPAC>2.0.CO;2)

Stampoulis, D., Anagnostou, E. N., and Nikolopoulos, E. (2013). Assessment of High Resolution Satellite-based Rainfall Estimates over the Mediterranean during Heavy Precipitation events. *Journal of Hydrometeorology*, 14(5), 1500-1514.

Tiedtke, M., (1989). A Comprehensive Mass Flux Scheme for Cumulus Parameterization in Large-Scale Models. *Mon. Wea. Rev.*, 117(8), 1779–1800. doi.org/10.1175/1520-0493(1989)117<1779:ACMFSF>2.0.CO;2.

Van Baelen, J., Reverdy, M., Tridon, F., Labbouz, L., Dick, G., Bender, M., and Hagen, M. (2011). On the relationship between water vapour field evolution and the life cycle of precipitation systems. *QJRMS*, 137(S1), 204–223. doi:10.1002/qj.785.

Wang, Q.-W and Xue, M. (2012). Convective initiation on the 19 July 2002 during IHOP: High-resolution simulations and analysis of the mesoscale structures and convective initiation. *J. Geophys. Res.*, 117, D12107.

Weckwerth, T. M., Wilson, J. W., and Wakimoto, R. M., (1996). Thermodynamic variability within the convective boundary layer due to horizontal convective rolls. *Mon. Wea. Rev.*, 124(5), 769–784.

Weckwerth, T. M., Wulfmeyer, V., Wakimoto, R. M., Hardesty, R. M., Wilson, J. W., and Banta, R. M. (1999). NCAR–NOAA Lower-Tropospheric Water Vapor Workshop. *Bull. Amer. Meteor. Soc.*, 80(11), 2339–2357.

Weckwerth, T.M. (2000). The effect of small-scale moisture variability on thunderstorm initiation. *Mon. Wea. Rev.*, 128(12), 4017-4030.

Weisman, M. L., Skamarock, W. C., and Klemp, J. B., (1997). The resolution dependence of explicitly modeled convective systems. *Mon. Wea. Rev.*, 125(4), 527–548.

Wernli, B. H. and Davies, H. C. (1997). A Lagrangian-based analysis of extratropical cyclones. I: The method and some applications. *QJRMS*, 123(538), 467–489. doi:10.1002/qj.49712353811.

Winschall, A., Pfahl, S., Sodemann, H., and Wernli, H. (2012). Impact of North Atlantic evaporation hot spots on southern Alpine heavy precipitation events. *QJRMS*, 138(666), 1245–1258. doi:10.1002/qj.987.

Winschall, A., Sodemann, H., Pfahl, S., and Wernli, H. (2014). How important is intensified evaporation for Mediterranean precipitation extremes? *J. Geophys. Res. Atmos.*, 119(9), 5240–5256. doi:10.1002/2013JD021175.

Figures

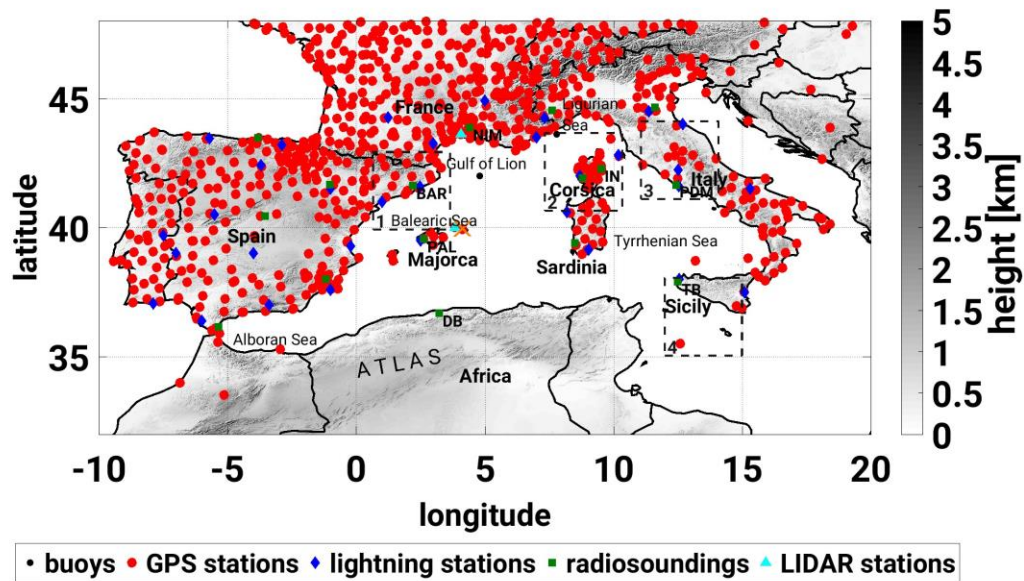
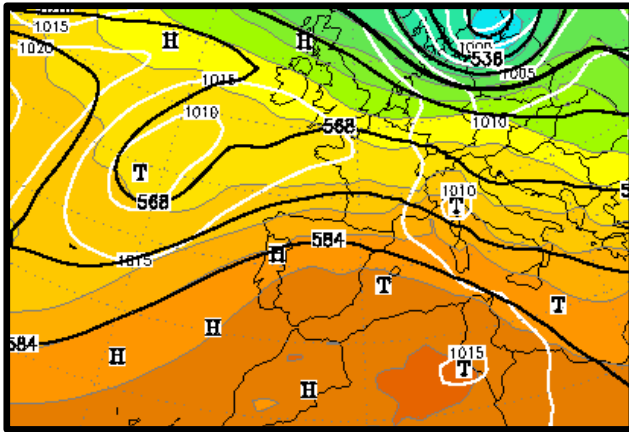
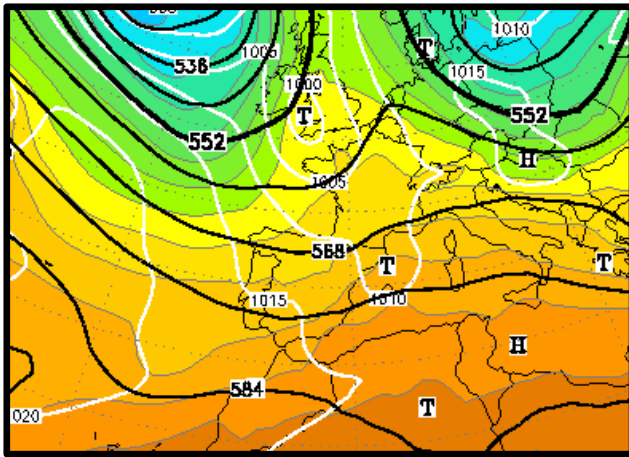


Figure 1: Orography of the western Mediterranean region (black-white scale). Subdomains under investigation are delineated with dashed lines and numbered from 1 to 4. Observations are indicated as follows: GPS network (red), radiosoundings (green), lightning stations (blue), buoys (black), WALI lidar and BASIL lidar (light blue); the orange cross over the south-eastern Menorca indicates the Boundary Layer Pressured Balloons (BLPB) launch site at the beginning of the balloon trajectories. Selected radiosounding stations are named as follows (from left to right) BAR (Barcelona), PAL (Palma), NIM (Nimes), IN (Inra), PDM (Pratica Di Mare) and TB (Trapani Birgi).

(a) 09.10.2012 1200 UTC



(b) 11.10.2012 1200 UTC



(c) 13.10.2012 1200 UTC

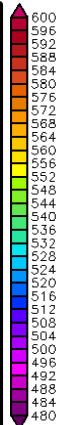
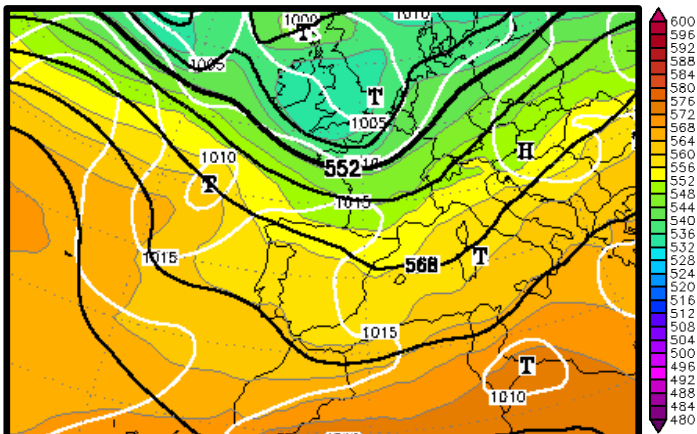
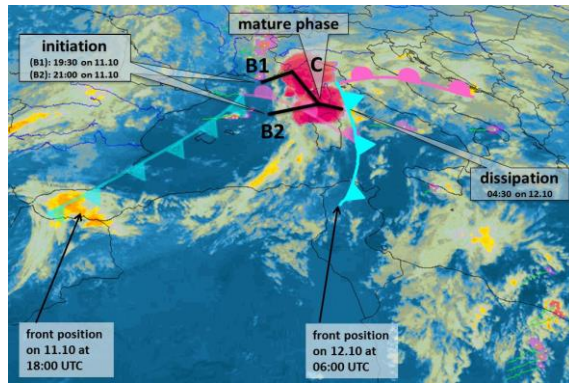
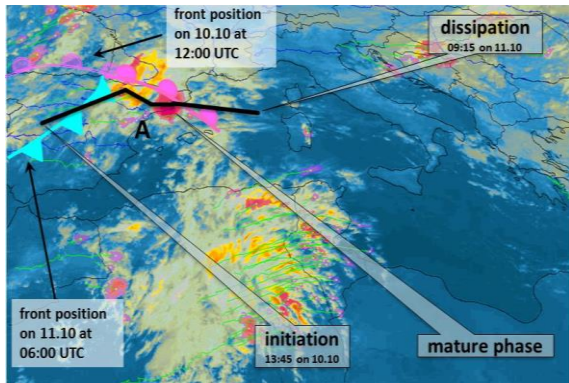


Figure 2: GFS-analysis of 500 hPa geopotential height (gpdgm; black isolines), mean sea-level pressure (hPa; white isolines) and relative topography H500-H1000 (gpdgm; colour scale) at 1200 UTC on the 9, 11 and 13 October 2012 (source: wetter3.de).

(a) 11.10.2012 at 0000 UTC

(b) 12.10.2012 at 0000 UTC



(c) 12.10.2012 at 0500 UTC

(d) 13.10.2012 at 1400 UTC

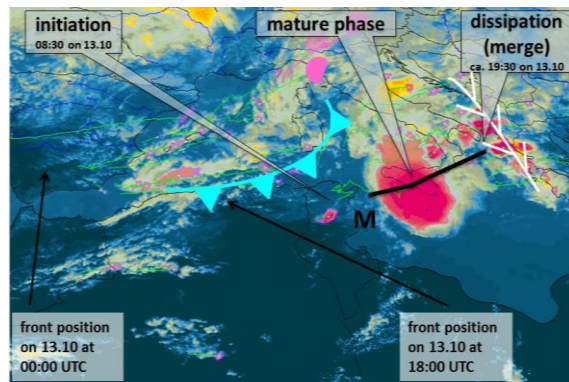
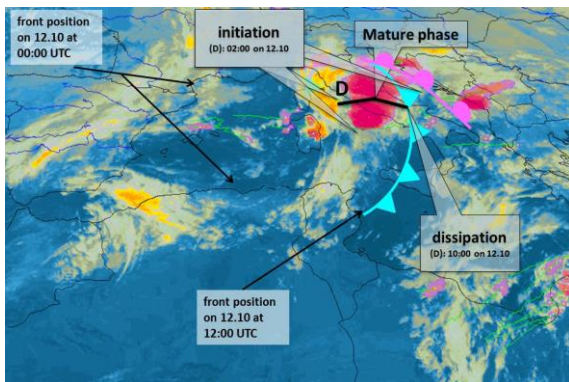
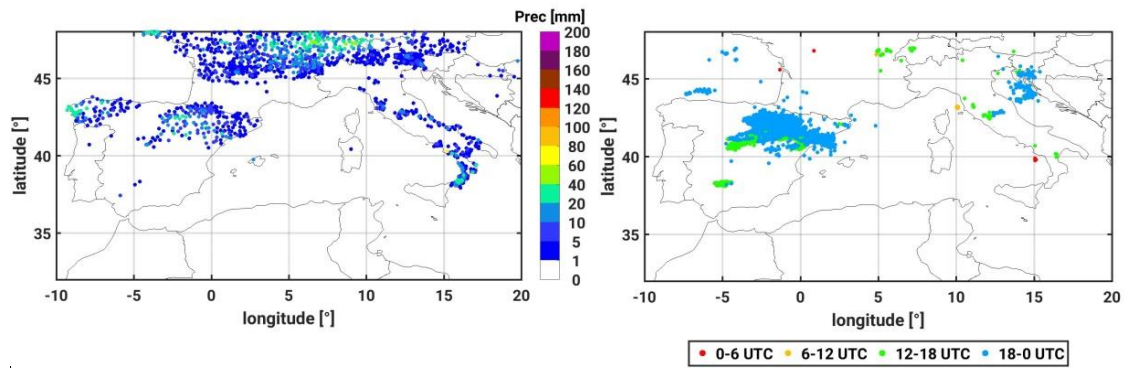
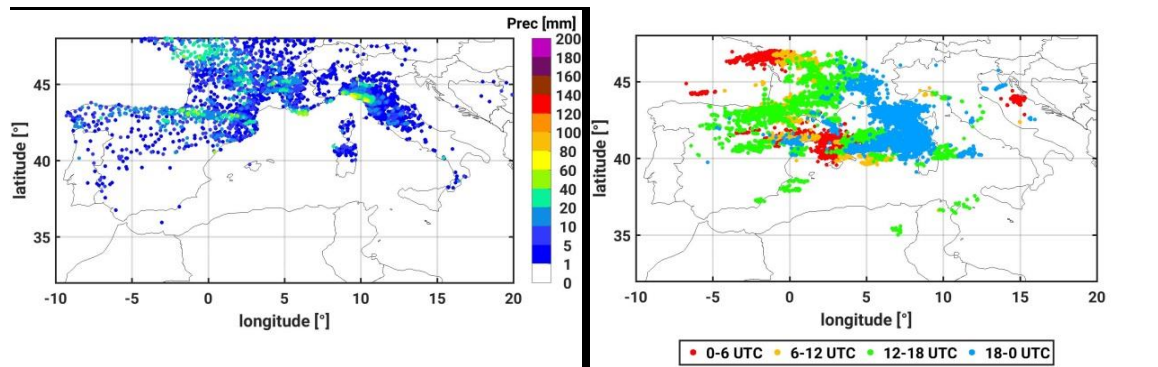


Figure 3: RDT (Rapid Developing Thunderstorm) products based on MSG SEVIRI brightness temperature images at 10.8 μm showing the spatio-temporal development of convective activity over the Mediterranean region for (a) 11 October 2012 at 0000 UTC, (b) 12 October 2012 at 0000 UTC, (c) 12 October 2012 at 0500 UTC and (d) 13 October 2012 at 1400 UTC. All development stages of storms are highlighted using different colours (yellow=triggering, orange=growing, magenta=mature stadium, violet= split cases). The blue, pink and white lines represent the position of fronts and convergence lines, respectively. The thick black lines locate the path of each storm and the captions indicate the stage of every convective cell.

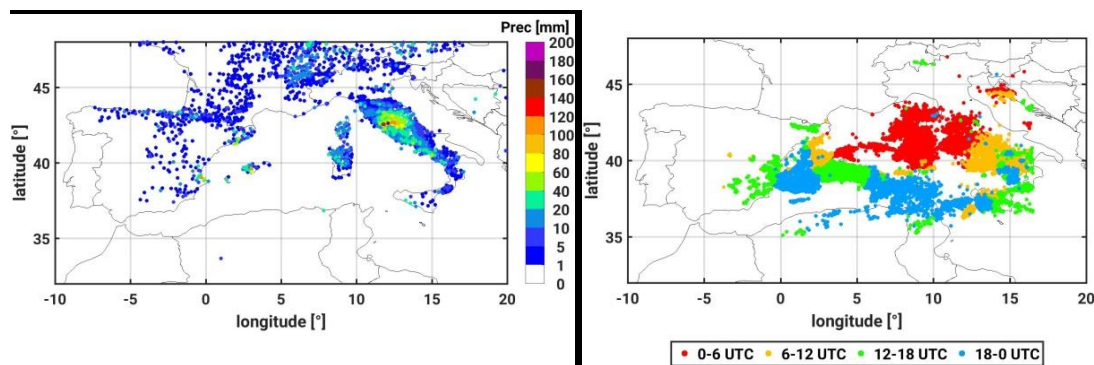
(a) 10.10.2012



(b) 11.10.2012



(c) 12.10.2012



(d) 13.10.2012

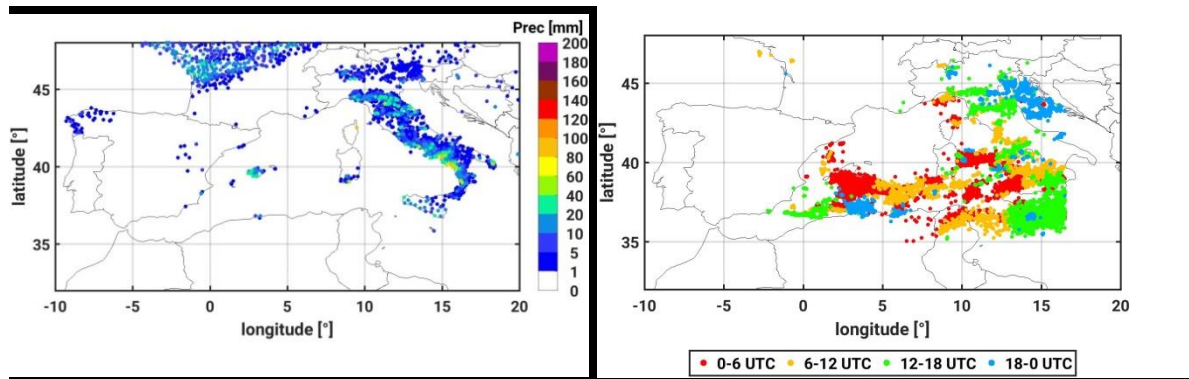
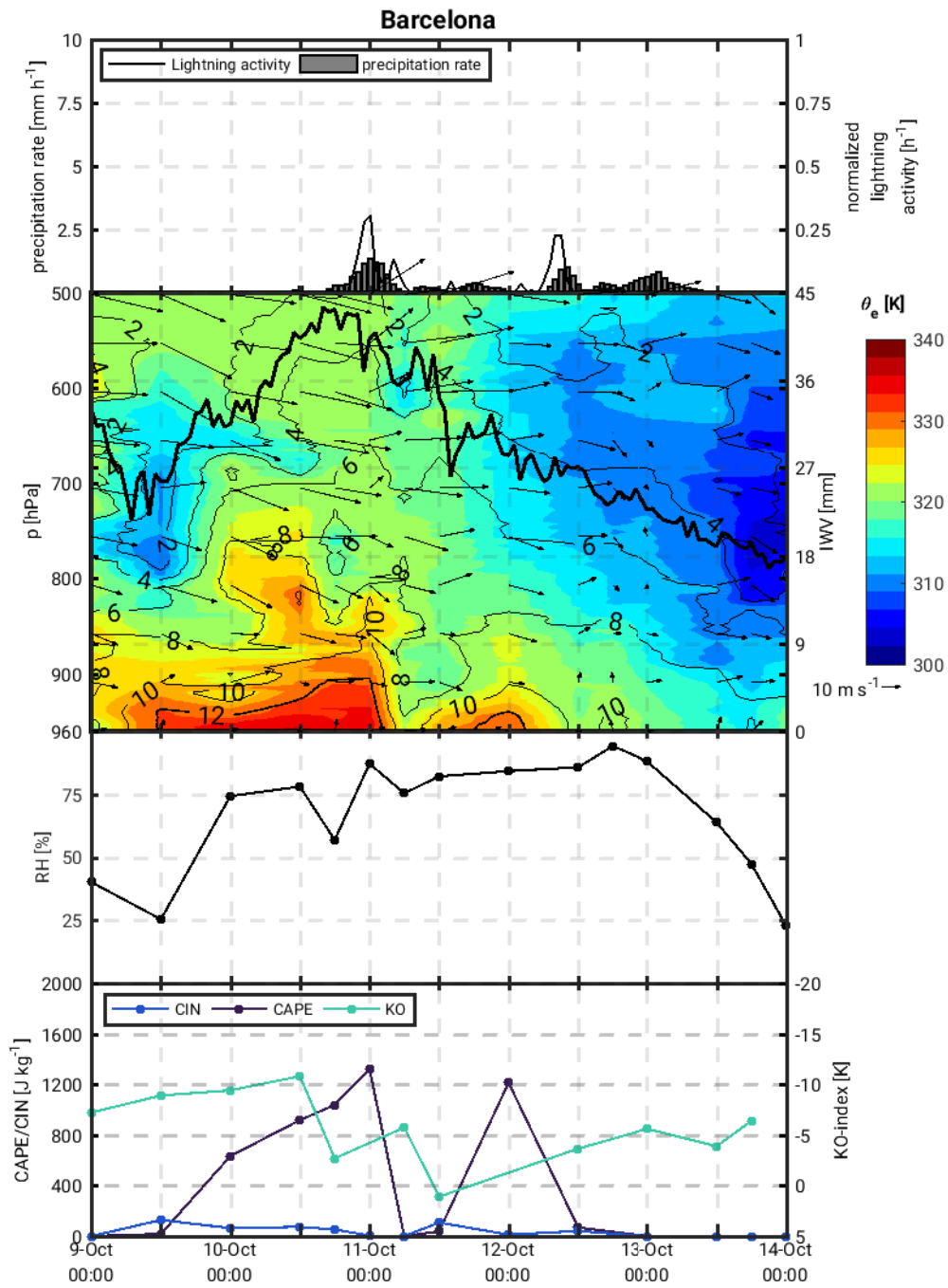
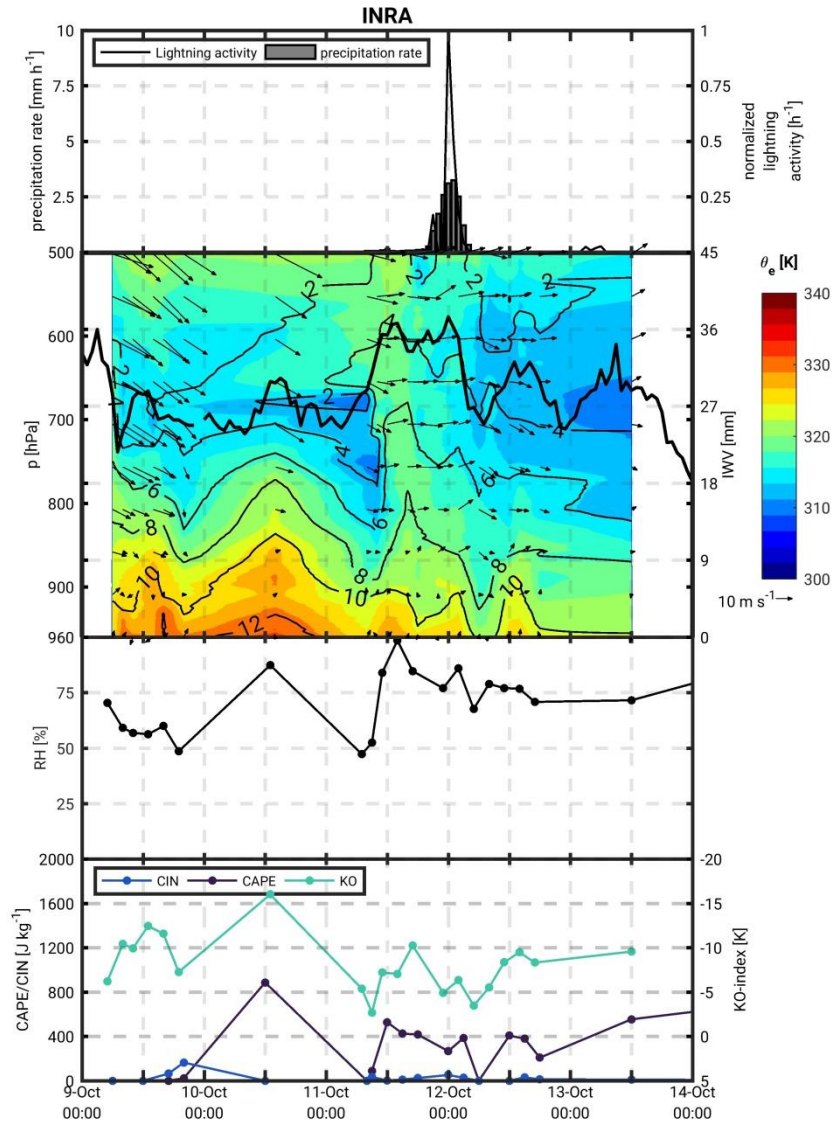


Figure 4: (a-d, left) Daily precipitation sums from 0600 UTC to 0600 UTC from 1 h rain gauge measurements and (right) EUCLID lightning observations (only available up to 16 °E).

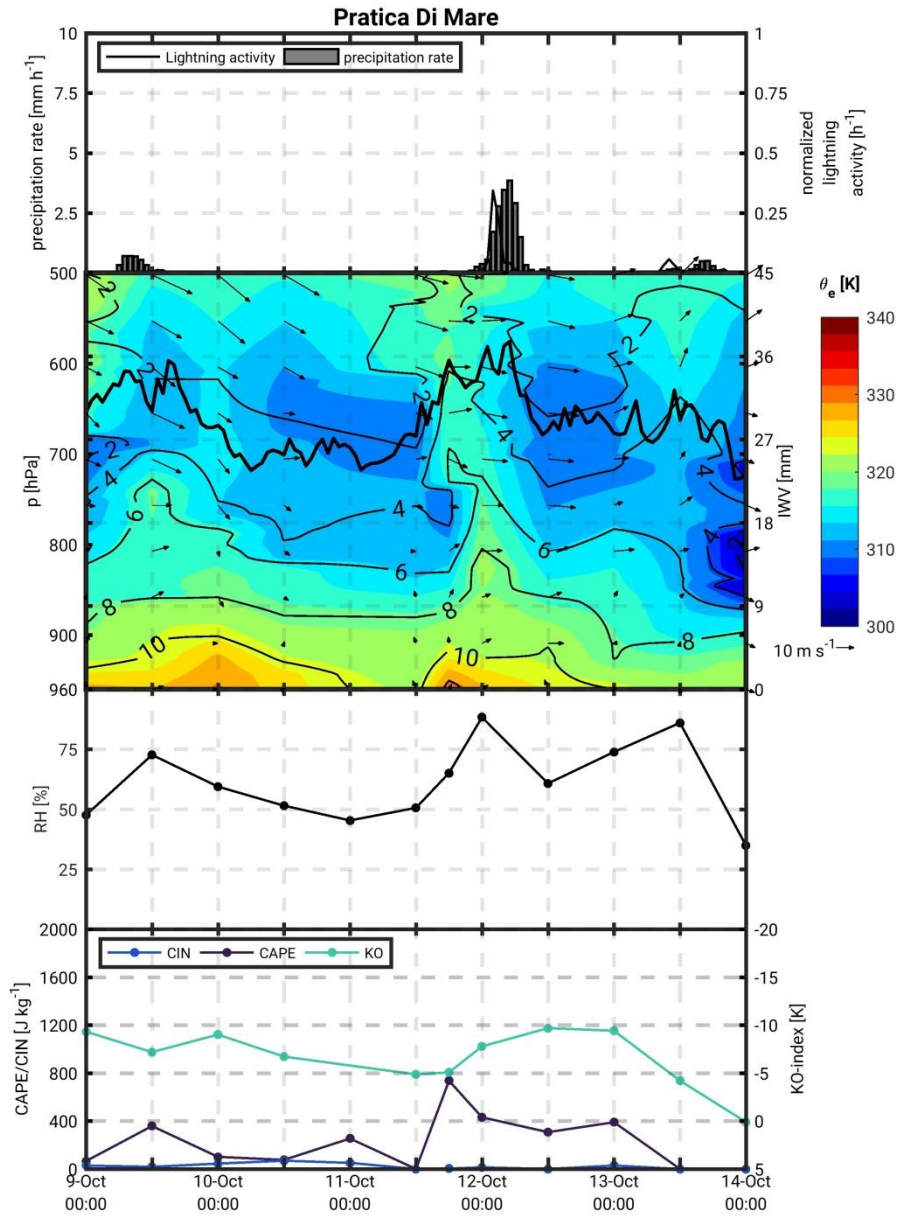
(a)



(b)



(c)



(d)

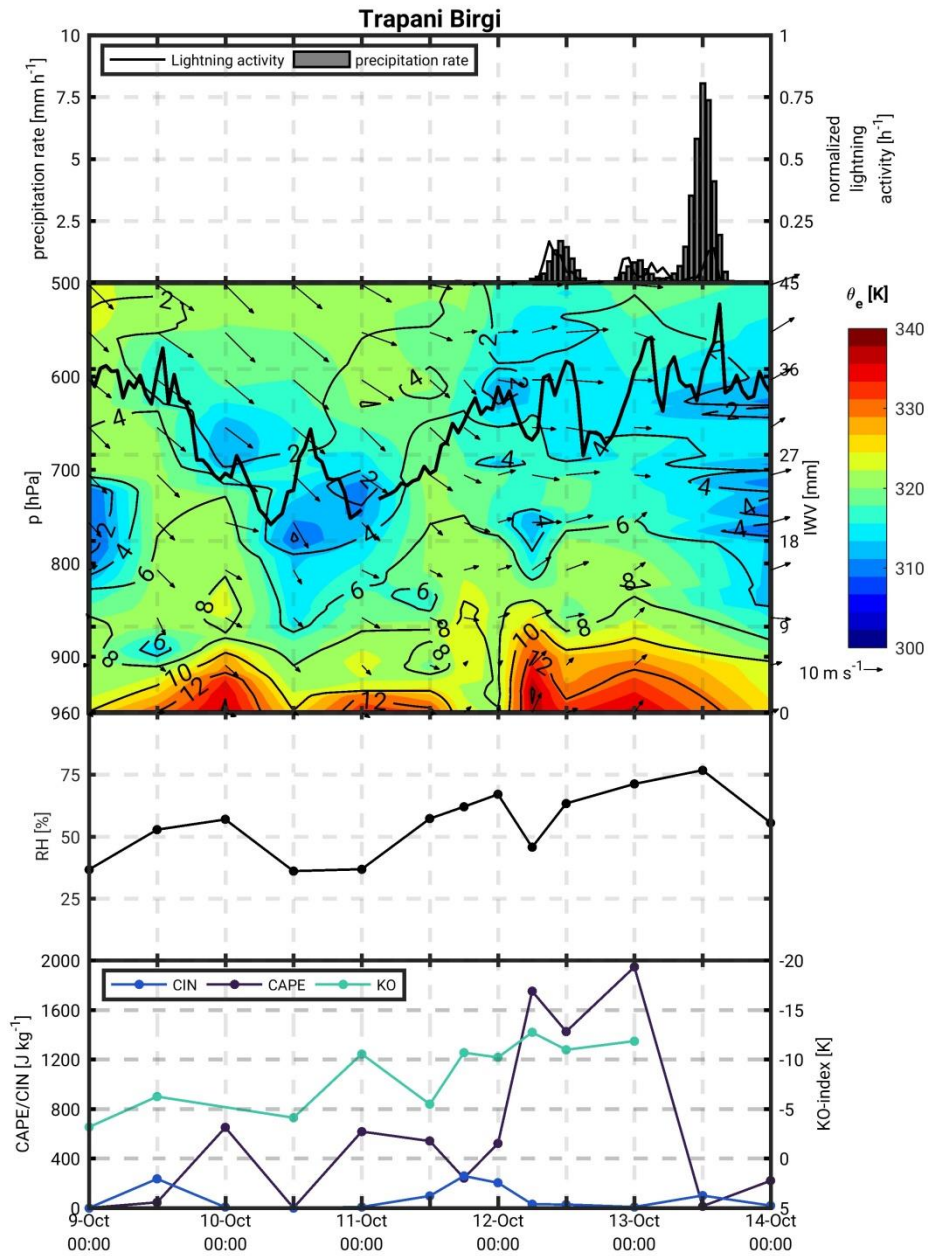


Figure 5: Temporal evolution of (from top to bottom): Areal mean CMORPH hourly precipitation observations and EUCLID lightning; vertical cross-sections of equivalent

potential temperature, specific humidity and horizontal wind (north pointing upwards) for selected stations using radiosounding data; IWV temporal evolution of the closest GPS station is included, mean relative humidity (RH) averaged between 850 and 700 hPa and temporal evolution of CAPE, CIN and KO-index calculated from corresponding radiosonde for: (a) Barcelona, (b) KIT-INRA, (c) Pratica Di Mare, (d) Trapani Birgi. Position of stations and selected areas are indicated in Figure 1.

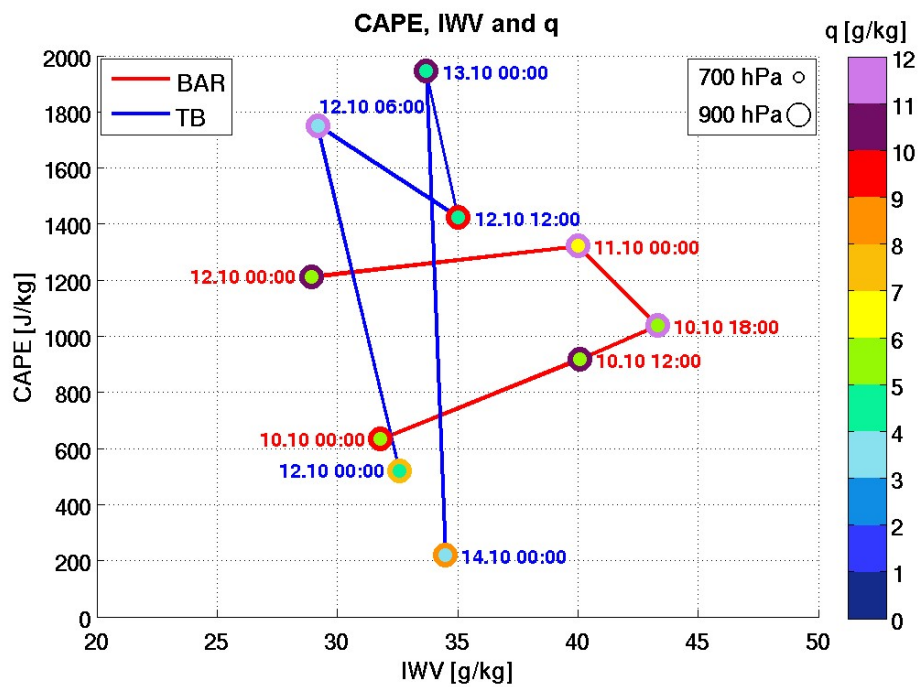
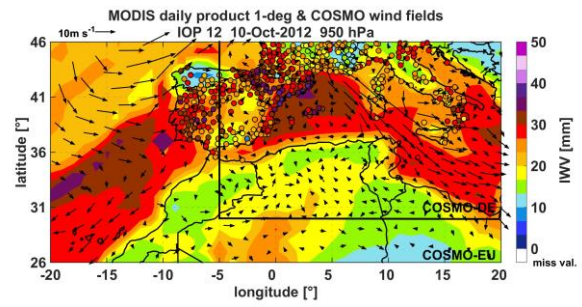
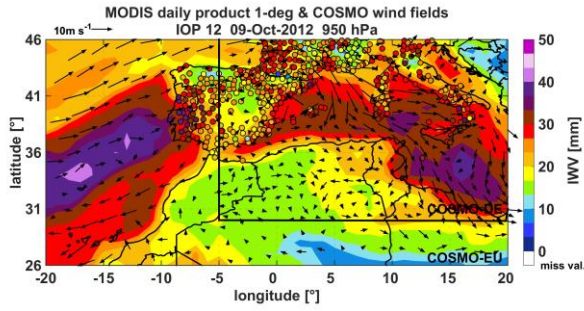


Figure 6: Temporal evolution of CAPE in relation to IWV and specific humidity at 900 ± 50 hPa and 700 ± 50 hPa using the Barcelona (BAR/AREA1; max prec ~ 50 mm day $^{-1}$ at about 11 October at 0000 UTC), and Trapani Birgi (TB/AREA4; max prec ~ 200 mm day $^{-1}$ in the morning of the 13 October) radiosounding atmospheric profile information. As indicated in the legend, the inner circle indicates the 700 hPa specific humidity values and the outer circle the 900 hPa specific humidity values.

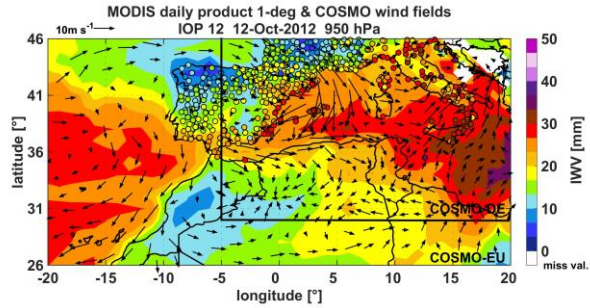
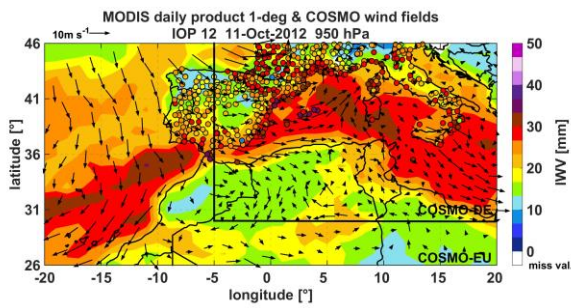
(a) 09.10.2012

(b) 10.10.2012



(c) 11.10.2012

(d) 12.10.2012



(e) 13.10.2012

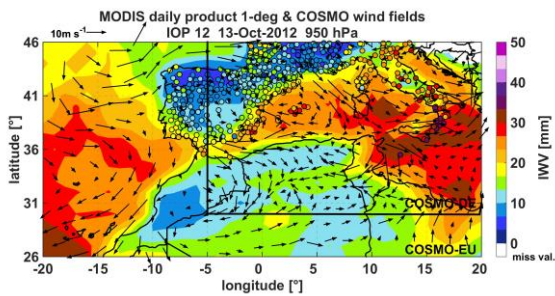
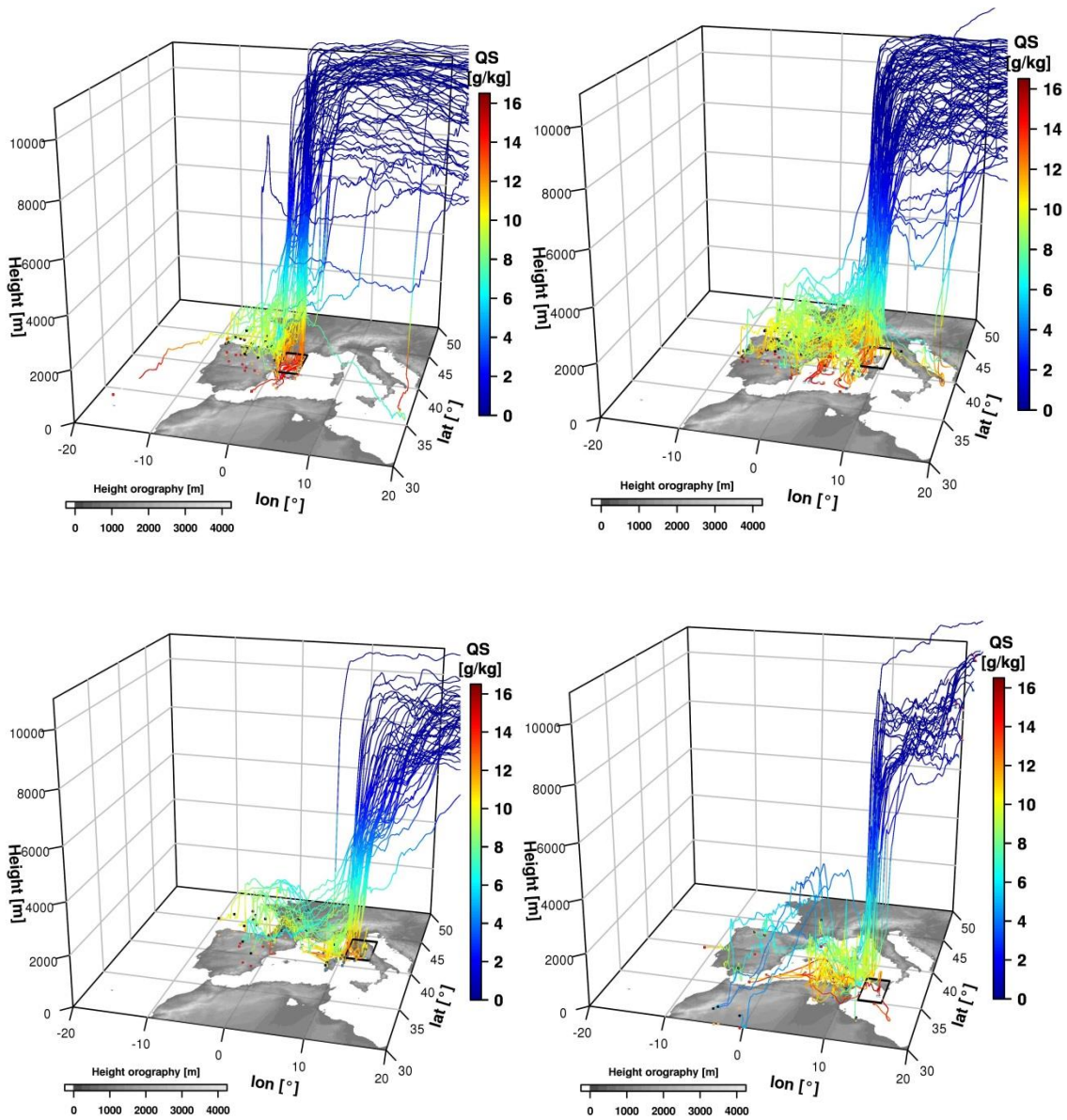


Figure 7: Daily mean spatial distribution of total column Integrated Water Vapour (IWV) from MODIS (background) and GPS (circles) observations for (a) 09 October 2012, (b) 10 October 2012, (c) 11 October 2012, (d) 12 October 2012 and (e) 13 October 2012. Simulated COSMO-7 km and COSMO-2.8km 950 hPa winds at 1200 UTC are superimposed.

(a)



(b)

This article is protected by copyright. All rights reserved.

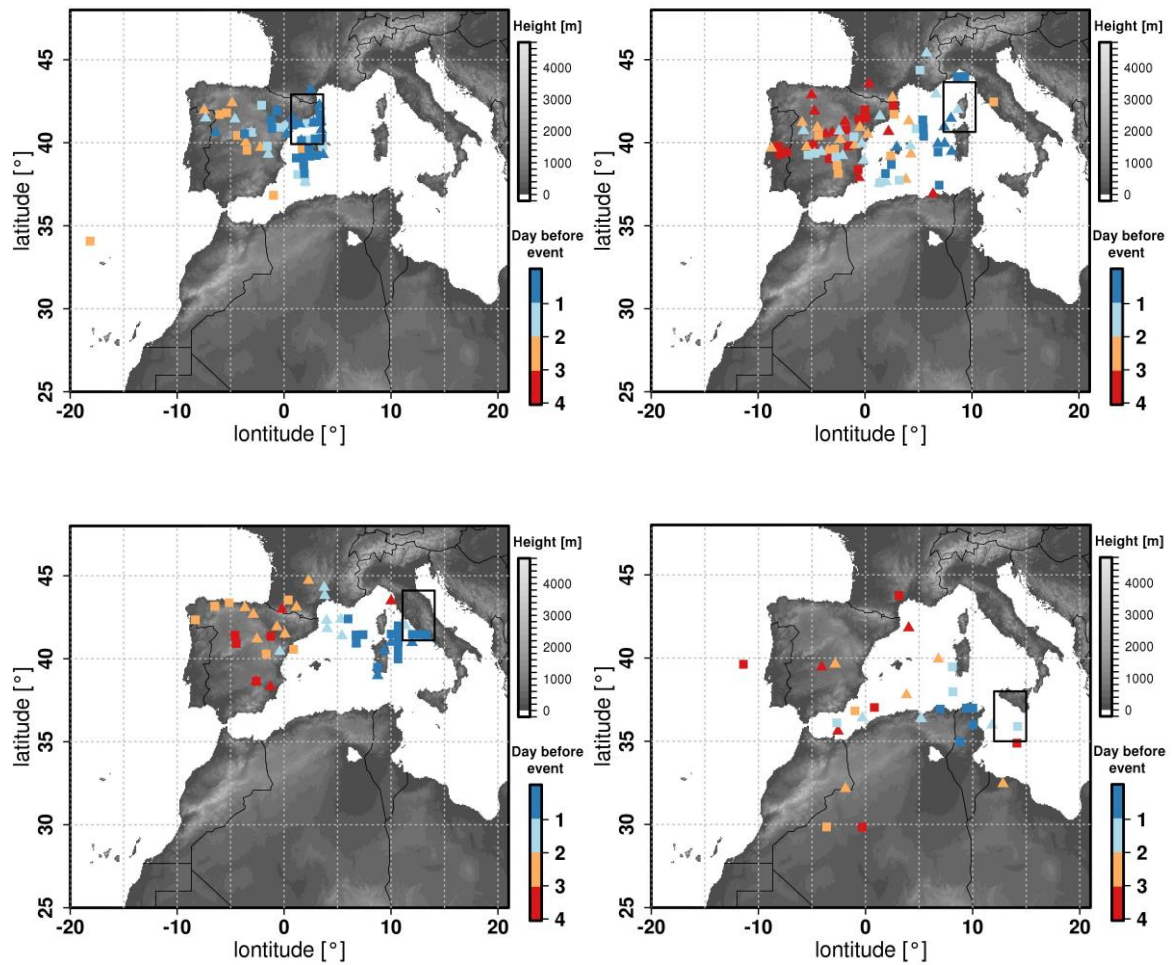


Figure 8: (a) Trajectory and (b) origin of air parcels contributing to the formation of the heavy precipitation systems in each of the affected areas (black boxes) as determined from the COSMO Lagrangian trajectories module. The orography of the region is depicted in white-black scale. In (a) the colour scale indicates the specific humidity along the air parcel trajectories. In (b) the symbols locate the origin of the air parcel trajectories and the colour scale indicates the number of simulated days prior to the precipitation event. The symbols themselves represent the starting time of trajectories (squares at 00UTC and the triangles at 12UTC).

(a)

(b)

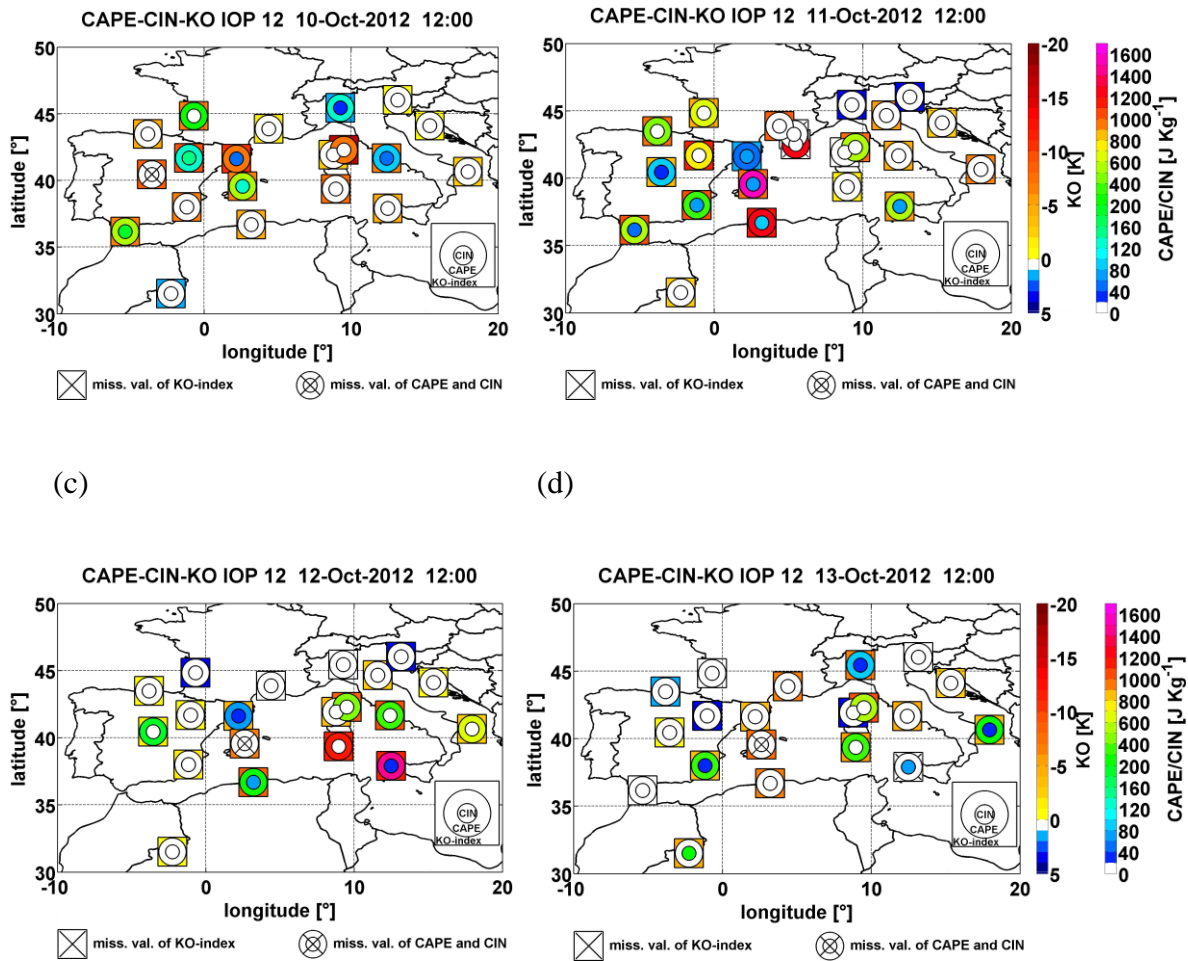
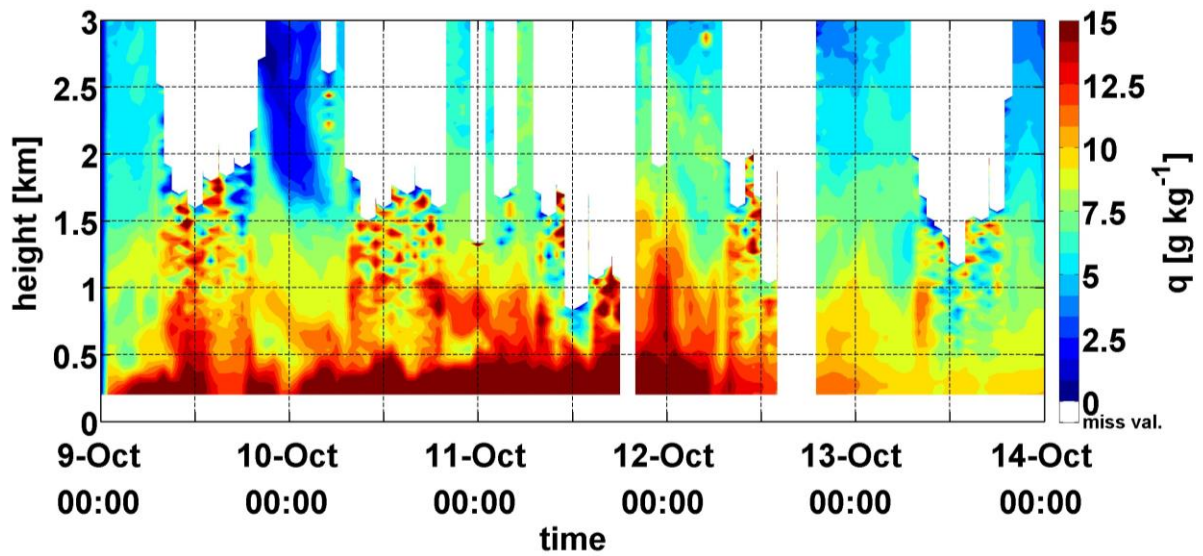


Figure 9: Spatial distribution of CAPE, CIN and KO-index on the 10, 11, 12 and 13 October 2012 at 1200 UTC. As indicated in the legend, the inner circle indicates CIN values, the outer circle represents the CAPE values, and the square reflects the KO-index values.

(a)



(b)

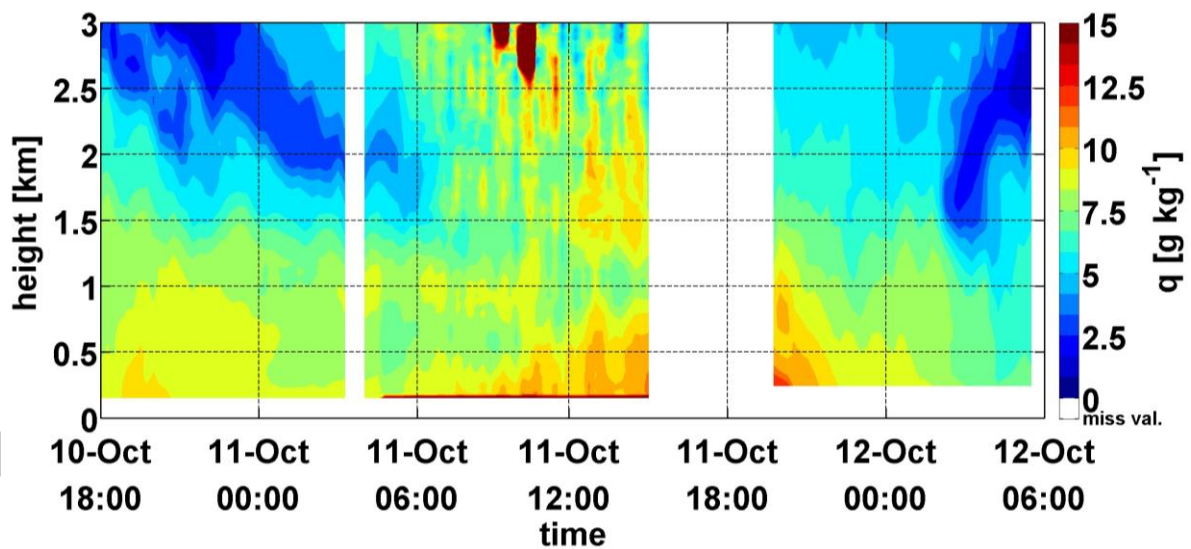
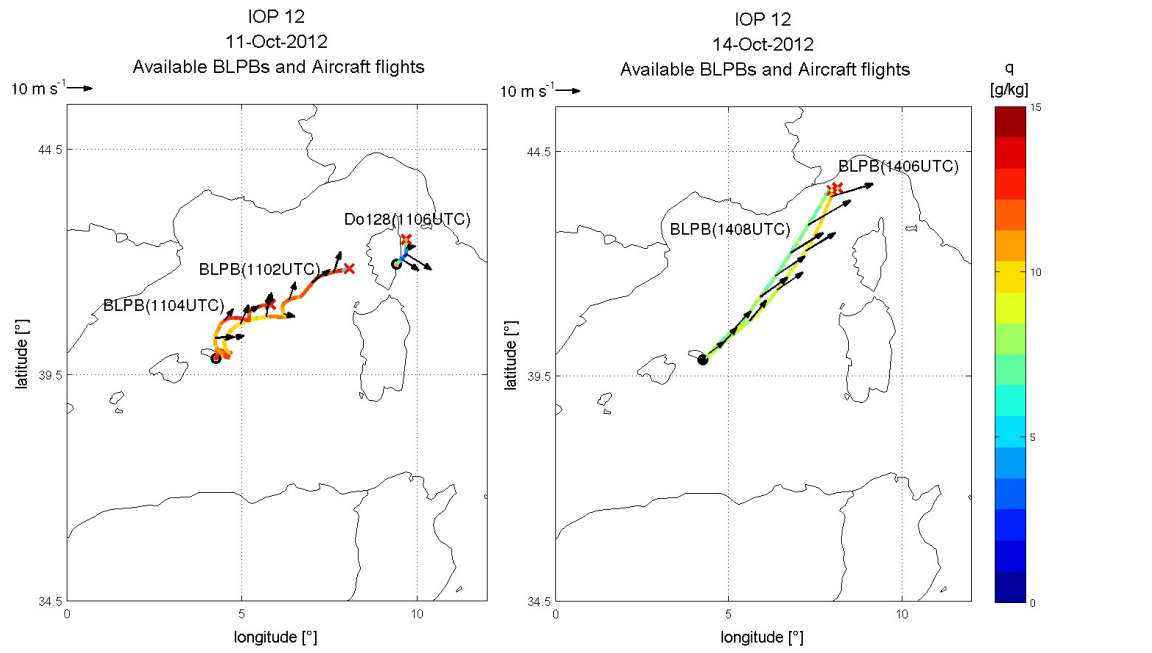
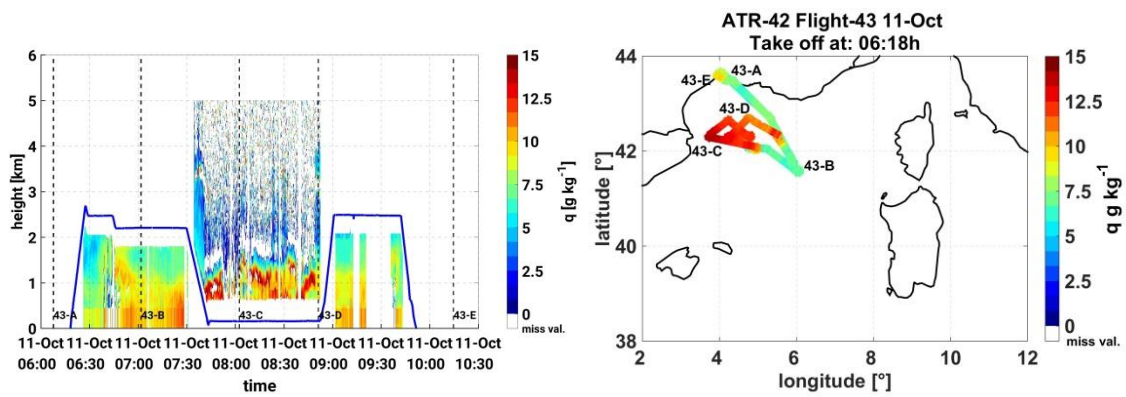


Figure 10: (a) Water vapour mixing ratio from 9 to 14 October 2012 over Menorca (Balearic Islands) as measured by the Raman lidar WALI. (b) Water vapour mixing ratio from 10 to 12 October 2012 over Candillargues (south France) as measured by the Raman lidar BASIL. Please note the different time scales. The data gaps are due to cloud cover or heavy rain.

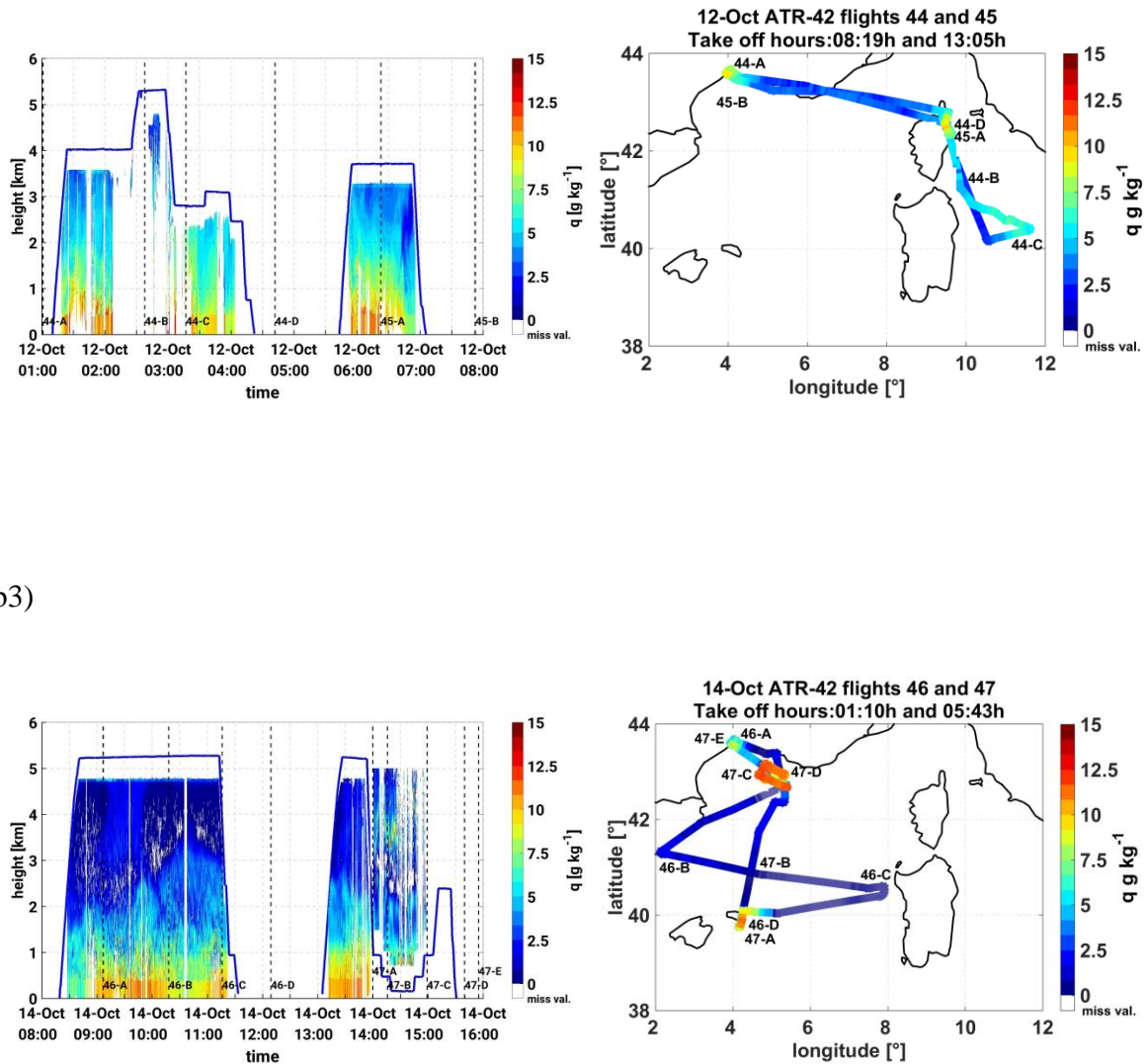
(a)



(b1)



(b2)



(b3)

Figure 11: (a) Boundary Layer Pressurized Ballons (BLPB) path depicting specific humidity and horizontal wind at about 500-700 m amsl on 11 October 2012 and 14 October 2012. DO-128 specific humidity and wind observations in the lower PBL for the 11 October are also included. (b) Vertical-cross section of specific humidity measured by the LEANDRE 2 lidar on board of the ATR-42 aircraft, on the 11, 12 and 14 October 2012 for the indicated periods. Flight tracks and altitude are also indicated.

Tables

Table 1: Complementary information on storms presented in Figure 3. The lifespan and maximum anvil surface were estimated based on information contained in the RTD product (accuracy is ± 15 min for the time estimates and ± 500 km² for maximum anvil expansion). Maximum precipitation amounts are inferred from rain gauge measurements over land and CMORPH satellite derived precipitation observations over the sea. Synoptic forcing information is based on GFS model output and surface pressure charts (source www.wetter3.de). Near-surface observations are based on SYNOP wind observations.

Storm	Lifespan [h]	Max. surface [x10 ³ km ²]	Max. prec [mm]	Forcing
A	19.5	39	50 /24h	Near-surface convergence line
B1	7	37	75/6h	Near-surface convergence line, secondary trough, surface cold front
B2	4.5	23	40/6h	
C (merged B1&B2)	4	130	50/24h	
D	8	93	150/6h	Near-surface convergence line, secondary trough, surface cold front
M	18	140	150-200/6h	Near-surface

				convergence line and secondary trough
--	--	--	--	--